Nuclear liquid-gas phase transition

M. Baldo[1] and L. S. Ferreira[1,2]
[1]*Istituto Nazionale di Fisica Nucleare, Sezione di Catania and Dipartimento di Fisica, Universitá di Catania, Corso Italia 57, I-95129 Catania, Italy*
[2]*Centro de Física das Interaccoẽs Fundamentais and Departámento de Física, Instituto Superior Técnico, Av. Rovisco Pais, 1096 Lisboa, Portugal*
(Received 8 June 1998)

The microscopic theory of the nuclear matter equation of state at finite temperature is developed within the Bloch–De Dominicis diagrammatic expansion. The liquid gas phase transition of symmetric nuclear matter is identified, with a critical temperature $T_c \approx 20$ MeV, using the Argonne v_{14} as the bare NN interaction and a phenomenological three-body force adjusted to give the correct saturation point. Pure neutron and asymmetric matter, relevant to supernovae explosions, are also studied. It is found that the liquid-gas phase transition disappears at asymmetries $a > 0.9$. At the bounce-off of the supernova collapse, temperatures of several tens of MeV are reached and we find that the compressibility steeply increases at such temperatures. Finally, we find that the equation of state gives a ''limiting temperature'' of finite nuclei consistent with the experimental observation in compound nucleus reactions. A careful analysis of the diagrammatic expansion reveals that the dominant terms are the ones that correspond to the zero-temperature Bethe-Brueckner-Goldstone diagrams, where the temperature is introduced in the occupation numbers only, represented by Fermi distributions, thus justifying this commonly used procedure of naively introducing the temperature effect.
[S0556-2813(99)04201-6]

PACS number(s): 21.65.+f, 26.50.+x, 26.60.+c, 25.70.−z

I. INTRODUCTION

The equation of state (EOS) of nuclear matter at finite temperature is of great interest in the physics both of heavy ion collisions and of supernova explosions. In recent experiments on heavy ion collisions at intermediate energies [1–3] the so-called ''caloric'' curve was determined. After selecting peripheral collisions, a quantity related to the temperature is defined through the yield of different light isotopes or the slopes of the light particle spectra. This quatity is then plotted as a function of the total excitation energy of the projectilelike fragments. In some cases [1] this plot presents a well-defined plateau, which is interpreted as evidence of a first order phase transition. Since nuclear matter is expected to undergo a liquid-gas phase transition, this can be taken as evidence of such a theoretical prediction. However, finite size effects and Coulomb corrections can drastically change the expectations based on infinite nuclear matter calculations. Indeed, the temperature at which the plateau is present, about 5–6 MeV, is much smaller than the critical temperature for the nuclear matter liquid-gas phase transition derived from Skyrme force models [4]. The plateau could actually be the evidence for a different type of instability [5,6]. In any case, the theoretical determination of the nuclear matter equation of state on a firm basis could be of great help in interpreting this set of experiments.

Concerning the astrophysical relevance, we can mention the latest stage of the supernova collapse, where the EOS of asymmetric nuclear matter at finite temperature plays a major role in determining the final evolution. The EOS is actually one of the most uncertain elements which enters in the collapse simulations.

Microscopic calculations of the nuclear EOS at finite temperature are quite few. The variational calculation by Friedman and Pandharipande [7] was one of the first few semimicroscopic investigation of the finite temperature EOS. The results appear fairly close to the predictions based on Skyrme force models: symmetric nuclear matter undergoes a liquid-gas phase transition, with a critical temperature $T_c = 18–20$ MeV. Different types of Skyrme forces give different critical temperatures, but they all lie close to this range of values. Later, Brueckner calculations at finite temperature [8] confirmed these findings with very similar values of T_c. The most recent calculations were presented in Ref. [9], where, however, a smaller value of T_c was found, $T_c \approx 10$ MeV. In Ref. [9] the full finite temperature formalism by Bloch and De Domicis [10] was followed. This discrepancy with previous calculations could be ascribed to the different nucleon-nucleon (NN) force used, to the improved many-body formalism, and finally to the different definition adopted for the single particle potential, as we will discuss in detail below.

In view of the fundamental relevance of the theoretical prediction of the nuclear EOS at finite temperature, up to the possible critical point, we have performed a systematic calculation of the EOS on the basis of the Bloch–De Dominicis formalism with a realistic NN interaction. Three-body forces (3BF's) were also introduced, since, as is well established [11], the phenomenological saturation point cannot be correctly reproduced with two-body forces only.

In Sec. II the finite temperature formalism by Bloch and De Dominicis is discussed in detail, in order to be used in the numerical applications. Three-body forces are described in Sec. III. The EOS at finite temperature is discussed in Sec. IV for symmetric nuclear matter, neutron, and asymmetric matter. In Sec. V, the limiting temperature of finite nuclei is studied along the nuclear stability line. Final conclusions are drawn in Sec. VI.

II. FINITE TEMPERATURE FORMALISM

A. Bloch–De Dominicis approach

The study of a many-body system at finite temperature, according to perturbation theory, has been developed by many authors along different lines. One can mention, for example, the finite temperature Green's function method, originally devised by Matsubara [12], the thermofield approach [13], and the Bloch–De Dominicis linked diagram expansion. The first one is more suited to the study of the single-particle properties of a many-body system. In this formalism the grand-canonical potential is expanded in irreducible connected diagrams involving an increasing number of finite temperature Green's functions and interactions. The expansion is therefore in the strength of the particle-particle interaction. For a system of strongly interacting particles and in presence of a hard core, like in nuclear matter, the convergence of the expansion is at least doubtful and it is difficult to select physically the relevant diagrams to be resummed.

The Bloch–De Dominicis (BD) expansion of the grand-canonical potential has the property to lead, in the zero-temperature limit, to the Bethe-Brueckner-Goldstone (BBG) expansion of the ground state energy. The latter is the expansion in the number of hole lines which univocally corresponds to the order of correlations considered. At the two-hole-line level the Brueckner approximation requires the introduction of a self-consistent single-particle potential [14,15]. At the three-hole-line level one gets the Bethe-Fadeev equations for the three-particle reaction matrix, which includes in the kernel the Brueckner two-body reaction matrix G. The hole expansion is expected to converge in nuclear matter, at variance with the expansion in the nucleon-nucleon interaction, since the G matrix can be viewed as a renormalized interaction in the medium, for which the effect of the strong core repulsion is largely reduced. Studies of the convergence of the expansion confirm this expectation [16].

The BD formalism nicely extends the BBG expansion to finite temperature, and therefore allows us to follow in a clear way the different contributions and their evolution with temperature. In this work we will adopt the BD formalism, which will be described in some detail in the following.

As in the BBG expansion at zero temperature, let us introduce an auxiliary single-particle potential U in such a way that the full nuclear Hamiltonian $H=H_0+v$ is rewritten as $H=H_0'+H_1$, with $H_0'=H_0+U$ and $H_1=v-U$, where v is the nucleon-nucleon interaction. The potential U has to be chosen in a way that use of the perturbation expansion in H_1 is justified. This means that in the perturbative expansion diagrams involving potential U insertions compensate higher order diagrams occurring in the original expansion of the interaction v. In this way the same expansion is rearranged with a greatly improved rate of convergence. Since the unperturbed Hamiltonian H_0' is still a one-body Hamiltonian

$$H_0'=\sum_k e_k a_k^\dagger a_k=\sum_k \left(\frac{\hbar^2k^2}{2m}+U(k)\right)a_k^\dagger a_k, \tag{1}$$

the perturbation expansion is the same as the one in terms of v, provided the single-particle spectrum is redefined as e_k and the so-called potential insertion diagrams are introduced. In Eq. (1) the operators a and $a^\dagger$ are the annihilation and creation operators for the single-nucleon state k, where the label k indicates the wave vector $\vec{k}$ and spin-isospin variables σ,τ.

The BD formalism is developed within the framework of the grand-canonical representation of statistical mechanics. The grand-canonical potential Ω is written as the sum of the unperturbed potential Ω_0' and a correlation term $\Delta\Omega$,

$$\Omega=\Omega_0'+\Delta\Omega, \tag{2}$$

corresponding to the one-body grand-canonical potential and a power series expansion in the interaction H_1 involving connected diagrams only, respectively. The unperturbed potential is defined by

$$\Omega_0'=\Omega_0-\sum_k U_k n(k), \tag{3}$$

with Ω_0 the grand-canonical potential of the independent particle Hamiltonian H_0', and the summation over U_k represents the first potential insertion diagram, to be discussed below. Therefore, Ω_0' includes all one-body correlations. The explicit form of the correlation term $\Delta\Omega$ is

$$\begin{aligned}\Omega-\Omega_0'=&\int_{-\infty}^{\infty}\frac{e^{-\beta\omega}}{2\pi}d\omega\sum_{p=1}^{\infty}(-1)^p\frac{i}{p}\mathrm{Tr}\left[e^{\beta\mu N}\left(H_1\frac{1}{H_0-\omega-i\epsilon}\right)^p\right]_c\\&-\int_{-\infty}^{\infty}\frac{e^{-\beta\omega}}{2\pi}d\omega\sum_{p=1}^{\infty}(-1)^p\frac{i}{p}\mathrm{Tr}\left[e^{\beta\mu N}\left(H_1\frac{1}{H_0-\omega+i\epsilon}\right)^p\right]_c\\=&\int_{-\infty}^{\infty}\frac{e^{-\beta\omega}}{2\pi}d\omega\sum_{p=1}^{\infty}(-1)^p\frac{2}{p}\mathrm{Im}\left\{\mathrm{Tr}\left[e^{\beta\mu N}\left(H_1\frac{1}{H_0-\omega+i\epsilon}\right)^p\right]_c\right\},\end{aligned} \tag{4}$$

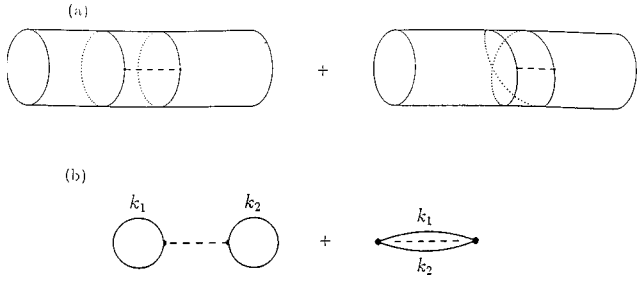

FIG. 1. The Hartree and Fock terms in the Bloch–De Dominicis (BD) finite temperature perturbation theory (a). The solid external lines represent particle propagation, while the dashed lines, joining two vertices (dots), represent the damped interaction of Eq. (5). The corresponding zero-temperature diagrams of the BBG expansion are depicted in (b).

where β is the inverse temperature $1/T$, μ the chemical potential, and N the total number of particle operator. The quantity ω is the energy integration variable. The symbol ''Im'' means imaginary part and the $\epsilon \to 0+$ limit has to be considered; finally, ''Tr'' indicates the trace operation. Formally this expression resembles closely the corresponding linked cluster expansion of the ground state energy in the zero-temperature case [17]. The trace can be calculated in terms of the finite temperature diagrams introduced by BD. These diagrams are also very similar to the zero-temperature Goldstone ones, with two main differences; namely, they are drawn on a cylindrical surface instead of a plane and all lines appearing in a diagram are particle lines. The need for this surface, instead of the usual plane, comes from the presence of the trace operation. Drawing a specific diagram on a plane surface leads to open diagrams where the entry and the exit external lines are labeled by the same momenta. This suggests naturally the idea of joining the lines with the same momentum, thus generating a cylindrical surface. The label c in Eq. (4) indicates that only connected diagrams must be included in the expansion, which is a consequence of the exponential formula for the partition function [10]. As an example, in Fig. 1(a) is depicted the first order diagrams, the Hartree-Fock terms, which corresponds to the zero-temperature diagrams of Fig. 1(b). The distinctive feature of the BD expansion is the appearance of the so-called ''spirals'' in the diagrams, lines which undergo one or more turns around the cylinder without being attached to any interaction. They correspond to a series of contractions between the creation operators defining the particle states, on the left and on the right of the interaction operator, whose trace is calculated. The whole set of diagrams can be generated by considering the diagrams without any spirals and adding to them the spirals in all possible combinations. The diagrams so obtained from a given original diagram without spirals can be summed up explicitly and it amounts to the introduction of a statistical factor $n_> = 1 - n(k)$, for each line labeled by the momentum k, $n(k)$ being the Fermi-Dirac distribution. It is therefore enough to consider only diagrams without any spiral and insert a factor $1-n$ in each line. This process is equivalent to the substitution of the original two-body interaction v with a ''damped'' interaction $\mathcal{V}$,

$$\begin{aligned}\langle k_1 k_2|v|k_3 k_4\rangle &\to \langle k_1 k_2|\mathcal{V}|k_3 k_4\rangle \\ &\equiv n_>(k_1)^{1/2} n_>(k_2)^{1/2} \langle k_1 k_2|v|k_3 k_4\rangle \\ &\quad \times n_>(k_3)^{1/2} n_>(k_4)^{1/2}. \end{aligned} \tag{5}$$

The trace expansion can therefore be rewritten in terms of the damped interaction. Restricting the summation to connected diagrams without spirals one obtains

$$\begin{aligned}\Omega - \Omega_0' = &\int_{-\infty}^{\infty} \frac{e^{-\beta\omega}}{2\pi} d\omega \sum_{p=1}^{\infty} (-1)^p \\ &\times \frac{2}{p} \mathrm{Im} \left\{ \mathrm{Tr} \left[e^{\beta\mu N} \left(\mathcal{V} \frac{1}{H_0 - \omega + i\epsilon} \right)^p \right]_{c,NS} \right\}, \end{aligned} \tag{6}$$

where the subscript NS means diagrams without spirals. It is noticeable that the only nontrivial dependence on the temperature is contained now in the factors $n_>$ of the damped interaction. The ω integration is equivalent to a contour integral in the complex plane which encloses the real axis counterclockwise. The use of this alternative representation in terms of a contour integral, instead of Eq. (6), is decided according to convenience.

Let us now discuss the contribution of two-body correlations to the grand-canonical potential. As in the zero-temperature Brueckner theory, one has to sum up the ''ladder'' series of diagrams. The first terms of the series is the Hartree term of Fig. 1, together with the exchange Fock term. The series continues with the terms depicted in Fig. 2. These pictures are assumed to include also the corresponding exchange diagrams. It turns out that the series can be formally summed up exactly, and one gets

$$\begin{aligned}\Omega - \Omega_0' &= \frac{1}{2} e^{2\beta\mu} \int_{-\infty}^{\infty} \frac{e^{-\beta\omega}}{2\pi} d\omega \sum_{n=1}^{\infty} \frac{(-)^n}{n} \\ &\quad \times \mathrm{Tr}_2 \{ [\mathcal{K}(\omega) \pi \delta(H_0 - \omega)]^{n-1} \}, \\ &= \frac{1}{2} e^{2\beta\mu} \int_{-\infty}^{\infty} \frac{e^{-\beta\omega}}{2\pi} d\omega \\ &\quad \times \mathrm{Tr}_2 \{ \arctan[\mathcal{K}(\omega) \pi \delta(H_0 - \omega)] \}, \end{aligned} \tag{7}$$

with the integer n restricted to odd values. The trace in the previous equation, Tr_2, is taken in the space of antisymmetrized two-body states and the two-body scattering matrix $\mathcal{K}$ is defined by

$$\begin{aligned}&\langle k_1 k_2|\mathcal{K}(\omega)|k_3 k_4\rangle \\ &\quad = [n_>(k_1) n_>(k_2) n_>(k_3) n_>(k_4)]^{1/2} \langle k_1 k_2|K(\omega)|k_3 k_4\rangle, \end{aligned} \tag{8}$$

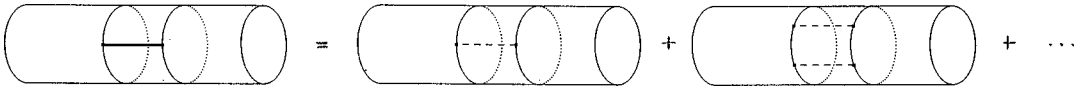

FIG. 2. Two-body ladder series in the BD expansion with the same notation as in Fig. 1.

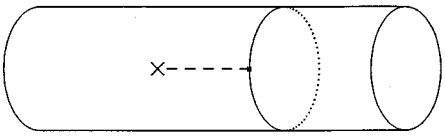

FIG. 3. The first potential insertion in the BD expansion. The cross indicates the auxiliary potential U.

where the scattering matrix K satisfies the integral equation

$$\langle k_1k_2|K(\omega)|k_3k_4\rangle = \langle k_1k_2|v|k_3k_4\rangle + \sum_{k_3'k_4'} \langle k_1k_2|v|k_3'k_4'\rangle \times \frac{n_>(k_3')n_>(k_4')}{\omega - e}\langle k_3'k_4'|K(\omega)|k_3k_4\rangle. \quad (9)$$

Equation (9) coincides with the Brueckner equation for the G matrix at zero temperature, if the single-particle occupation numbers are taken at $T=0$. It has to be noticed that only the principal part has to be considered in the integration, thus making K a real matrix. This expression is the most straightforward generalization of the Brueckner G matrix at finite temperature, in the sense that the only modification is the temperature dependence in the Fermi function $n_>$. In Eq. (7) the temperature dependence is more involved. However, if one considers the first term in the expansion of the arctan function, it reduces to

$$\Omega_1 = \frac{1}{2}\sum_{k_1k_2} n(k_1)n(k_2)\langle k_1k_2|K(\epsilon_{k_1}+\epsilon_{k_2})|k_1k_2\rangle_A, \quad (10)$$

which defines the grand-canonical potential in total analogy with the BBG binding potential. The explicit forms both of the complete expression of Eq. (7) and of the first order term of Eq. (9) are given also in Appendix A.

It is necessary to discuss now the choice of the single-particle auxiliary potential U. First of all, the use of the ''continuous'' [18] choice is somehow mandatory, since at finite temperature there is no longer a sharp distinction between particle and hole states. In the original BD work, it was suggested to introduce a single-particle potential, in such a way that the first order potential insertion is just equal to minus twice the contribution of the ladder sum, in analogy with the Brueckner zero-temperature case. However, one can consider a general potential U and the first potential insertion of Eq. (3), as depicted in Fig. 3. In the zero-temperature case this potential insertion contribution cancels out exactly the potential part of the single-particle contribution coming from H_0', irrespective of the particular choice of U, as will be discussed in Sec. II C.

In the zero-temperature case, the choice of the single-particle potential for $k<k_F$ is such that the potential insertion diagram in the lower part of Fig. 4(b) cancels out exactly the three-hole ''bubble diagram'' in the lower part of Fig. 4(d). This is actually possible in virtue of the Bethe-Brandow-Petschak (BBP) theorem [19], which ensures that the G matrix appearing in the self-energy insertion in the hole line of Fig. 4(d) can be taken on shell. This choice is therefore equivalent to the definition

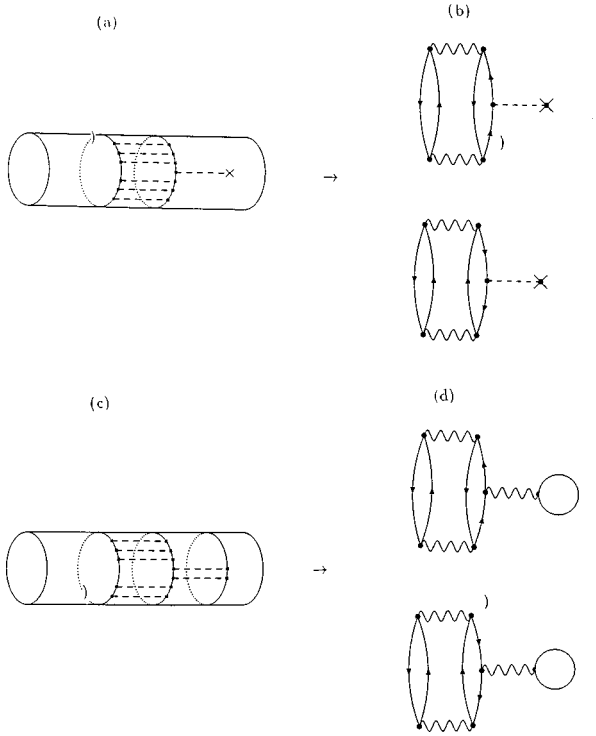

FIG. 4. Generic potential insertion diagram with two particle lines (a), which reduces to the hole and particle potential insertion diagrams of the BBG expansion at zero temperature depicted in (b). Generic three-particle-line diagram in the BD expansion (c) which reduces to the hole and particle bubble diagram in the BBG expansion (d).

$$U(\mathbf{k}_1) = \sum_{\sigma\tau}\sum_{\mathbf{k}_2}\langle k_1k_2|G(\omega)|k_1k_2\rangle_A\Theta_F(|\mathbf{k}_2|), \quad (11)$$

where $\Theta_F(|\mathbf{k}_2|)=1$ for $k<k_F$ and zero otherwise. This suggests, at finite T, an alternative definition of $U(k)$ in terms of K,

$$U(\mathbf{k}_1) = \sum_{\sigma\tau}\sum_{\mathbf{k}_2}\langle k_1k_2|K(\omega)|k_1k_2\rangle_A n(k_2). \quad (12)$$

This is also consistent with the natural interpretation of the K matrix, as the scattering matrix in the medium at finite temperature. One can indeed see that the mentioned cancellation between the bubble diagram and the potential insertion diagram of Fig. 4 is still valid at finite temperatures, once the single-particle potential of Eq. (12) is adopted.

According to the general expansion of Eq. (6), a general diagram of order p has the structure of a trace, with p damped interactions $\mathcal{V}$ and energy denominators. Furthermore, the energy integration has to be taken along the real axis. Of special interest are the diagrams which correspond to the ones appearing in the zero-temperature BBG expansion, where the Fermi step function is replaced by the finite temperature Fermi distribution $n(k)$. This set of finite temperature diagrams can be called the ''naive'' finite temperature BBG (NTBBG) expansion, in the sense that the tem-

perature enters only in a straightforward way through the extension of the Fermi function to finite temperature. In general, these diagrams are expected to be the dominant ones, since all the others contain at least one factor $n(k)n_>(k)$, which is small, especially at temperatures not too high. This will be clearly seen below, in the case of the finite temperature Brueckner-Hartree-Fock approximation, which includes the two-body correlations.

The same happens indeed, in the case of the diagrams of Fig. 4, which are the diagrams involved in the cancellation between the single-particle insertion and the bubble diagram. Figure 4(a) indicates the lowest order diagram with one potential insertion. The explicit expression reads

$$
\begin{aligned}
D_U=&\frac{i}{2}\int_C \frac{e^{-\beta\omega}}{2\pi}d\omega\sum_{\{k\}}\sum_p (-1)^p \\
&\times\frac{1}{p}\frac{\langle k_1k_1{}'|\mathcal{V}|k_2k_2{}'\rangle}{e_{k_2}+e_{k_2{}'}-\omega}\frac{\langle k_2k_2{}'|\mathcal{V}|k_3k_3{}'\rangle}{e_{k_3}+e_{k_3{}'}-\omega} \\
&\times\cdots\langle k_mk_m{}'|\mathcal{V}|kk'\rangle\frac{U(k')}{(e_k+e_{k'}-\omega)^2} \\
&\times\frac{\langle kk'|\mathcal{V}|k_{m+1}k_{m+1}{}'\rangle}{e_{k_{m+1}}+e_{k_{m+1}{}'}-\omega}\frac{\langle k_{m+1}k_{m+1}{}'|\mathcal{V}|k_{m+2}k_{m+2}{}'\rangle}{e_{k_{m+2}}+e_{k_{m+2}{}'}-\omega} \\
&\times\cdots\frac{\langle k_{p-1}k_{p-1}{}'|\mathcal{V}|k_1k_1{}'\rangle}{e_{k_1}+e_{k_1{}'}-\omega},
\end{aligned}
\tag{13}
$$

where C indicates the contour integration in the complex plane around the real axis. Apparently, this integral receives contributions from the first order singularities of the energy denominators of the ladder series, as well as from the double poles of the quadratic energy denominator. Using the residue theorem, one can check that the first set of poles gives rise to the following result:

$$
\begin{aligned}
D_U^{(1)}=&\frac{1}{2}\sum_{\{k\}} \\
&\times\frac{\langle k_1k_1{}'|K|kk'\rangle n_>(k)U(k')n_>(k')\langle kk'|K|k_1k_1{}'\rangle}{(e_k+e_{k'}-e_{k_1}-e_{k_1{}'})^2} \\
&\times n(k_1)n(k_1{}'),
\end{aligned}
\tag{14}
$$

where we have summed up the ladder series to get the scattering matrix of Eqs. (8) and (9), and used the identity $e^{-\beta(e_{k_1}-\mu)}n_>(k_1)=n(k_1)$. The contribution $D_U^{(1)}$ coincides with the zero-temperature diagram of the upper part of Fig. 4(b), except that each one of the Fermi step functions are now replaced by the finite temperature distribution.

Analogously, one finds that the contribution $D_U^{(2)}$ coming from the double pole corresponds to the lower diagram of Fig. 4(b), that is, to the hole potential insertion,

$$
\begin{aligned}
D_U^{(2)}=&\frac{1}{2}\sum_{\{k\}} \\
&\times\frac{\langle k_1k_1{}'|K|kk'\rangle n(k)U(k')n(k')\langle kk'|K|k_1k_1{}'\rangle}{(e_k+e_{k'}-e_{k_1}-e_{k_1{}'})^2} \\
&\times n_>(k_1)n_>(k_1{}').
\end{aligned}
\tag{15}
$$

A closer inspection of the analytical form of Eq. (13) shows actually that other contributions can appear, originated by possible double or higher poles coming from the possible energy degeneracies of the denominators. These corrections give rise to other finite temperature diagrams, which vanish at zero temperature since they contain factors $nn_>$, as discussed above. They are expected to be a minor correction at not too high temperature and not too low densities. This is true for all diagrams belonging to this set, with the exception of the ones describing the shift in the chemical potential [20], which do not vanish indeed, in the zero-temperature limit. The latter are included in our self-consistent procedure [21].

The simplest three lines diagrams, without U insertion, are depicted in Fig. 4(c). They represent a set of three-particle diagrams with an arbitrary number of ladder interactions between the two pairs of particles. Proceeding along the same lines, one can show that they introduce the diagrams of Fig. 4(d), which are the particle and hole bubble diagrams of the BBG expansion, again with the temperature Fermi distributions replacing the step functions. The previous considerations about higher pole contributions also applies for the particle bubble diagram.

As in the case of zero temperature, the lower diagrams of Figs. 4(b) and 4(d) cancel each other, which justifies the choice of Eq. (11) for the single-particle potential. We will see, anyhow, that this choice will differ in practice only little from the BD choice.

Equations (9) and (12) have to be solved self-consistently for the single-particle potential U, and for a fixed chemical potential and temperature. This can be achieved, in principle, with an iterative procedure as in the case of zero temperature.

Three-body or higher order correlations could, in principle, be treated along the same lines, even if the theory is not yet formally developed. However, there is strong evidence that the ''continuous'' choice for U is able to incorporate most of the higher order contributions at zero temperature [22], at least up to densities a few times larger than saturation. It can be expected that this holds true also at finite temperature, and therefore we will restrict all the calculations up to two-body correlations only.

As shown in Appendix A, the grand-canonical potential for symmetric nuclear matter can be written as

$$
\Omega=\Omega_0'+\Delta\Omega,
\tag{16}
$$

where

$$
\begin{aligned}
\frac{\Omega_0'}{V}\equiv&\,\omega_0' \\
=&-\frac{2}{\pi^2}\int_0^{+\infty}k^2dk\left[\frac{1}{\beta}\ln(1+e^{-\beta(e_k\mu)})+U(k)n(k)\right]
\end{aligned}
\tag{17}
$$

and μ the chemical potential. The interacting part of the grand-canonical potential is given explicitly by

$$\frac{\Delta\Omega}{V}\equiv\Delta\omega=\frac{2}{(2\pi)^3}\sum_{lSJT}\hat{J}^2\hat{T}^2\int dq\int P^2dPe^{-\beta(\overline{E}_{Pq}-2\mu)}\times d(q,P)\arctan\left[\frac{\pi[ql|K^{SJT}(\overline{E}_{Pq})|ql]q^2\overline{Q}(q,P)}{d(q,P)}\right], \tag{18}$$

where the density of state d is given by

$$d(q,P)=\left|\frac{\partial\overline{E}_{qP}}{\partial q}\right|=\left|\frac{2\hbar^2q}{m}+\frac{\partial}{\partial q}\overline{U}_{qP}\right|. \tag{19}$$

The two-particle energy $\overline{E}_{qP}$, the Pauli operator $\overline{Q}_{qP}$, and the potential felt by two particles $\overline{U}_{qP}$, are all angle averaged quantities, as explained in Appendix A. These angle averages are common in BBG calculations and are expected to be accurate, allowing us to make the contribution of different channels additive, since, then, only the diagonal part of K contributes. In practice, these angle averages are not needed for the first term of Eq. (10), and they will be used only in the evaluation of the higher order contribution. The quantum numbers $lSJT$ specify the two-body channel and $\hat{A}=\sqrt{2A+1}$.

B. Thermodynamical quantities

Once the grand-canonical potential is obtained, the pressure $\tilde{p}$ is immediately extracted, in principle, from the relation $\tilde{p}=-\omega\equiv-\Omega/V$. The latter gives the pressure as a function of the temperature T and the chemical potential μ, which can be considered the searched EOS. Then the density ρ could be extracted from the relation $\rho=-\partial\Omega/\partial\mu$. However, it has been found [23] that this procedure leads to numerical instability. To overcome this difficulty, one can start from the density and fix the chemical potential $\tilde{\mu}$ from the relation

$$\rho=\sum_k n(k)=\sum_k\frac{1}{e^{\beta(e_k-\tilde{\mu})}+1}, \tag{20}$$

which is an implicit equation for the chemical potential. This equation is mainly a mean field approximation for the density, and therefore the corresponding chemical potential is denoted by $\tilde{\mu}$, in order to be distinguished from the exact one μ. This equation is solved at each step of the iterative procedure with Eqs. (9) and (12). In general, this mean field relation is not fully consistent with the one derived directly from the grand-canonical potential, which contains also the contribution from two-body correlations. It is expected, therefore, that this inconsistency leads to a violation of some of thermodynamical equalities. Indeed, one finds in particular that the pressure $\tilde{p}$ extracted directly from the grand-canonical potential, as mentioned above, does not coincide with the pressure extracted from $p=\rho^2\partial f/\partial\rho$, where f is the free energy per particle. As discussed in Appendix B, this discrepancy expresses a violation of the generalized Hugenholtz–Van Hove theorem [24]. Physical arguments, as shown in the same appendix, suggest that the correct procedure is the one involving the free energy. In the practical calculations we then adopt the following procedure. For a given density and temperature we solve the self-consistent equations along with the Eq. (20) for the chemical potential, and obtain the grand-canonical potential ω. Finally we extract the free energy per particle f from the relation

$$f=\omega\rho+\tilde{\mu}. \tag{21}$$

The pressure is calculated performing a numerical derivative of f.

A derivation is often found in the literature for both the grand-canonical potential and the free energy, in which one calculates directly the internal energy E by extending the Brueckner expression to finite temperature within the ''naive'' TBBG expansion. Then, for the entropy $S=S(T,\tilde{\mu})$, the mean field approximation is used:

$$S=-\sum_k\{n(k)\ln n(k)+[1-n(k)]\ln[1-n(k)]\}. \tag{22}$$

The total free energy is then given by $F=E-TS$, and the grand-canonical potential $\Omega=F-\tilde{\mu}N$, where N is the total number of particles. This procedure mainly neglects the effect of the two-body correlations on the entropy and the higher order terms of the arctan expansion in the expression for the grand-canonical potential, Eq. (18). A comparison of the two methods is discussed in the following.

Using instead the formalism developed in Sec. II A, the entropy can be extracted, once the free energy is obtained from Eq. (21), by the standard relation

$$S(N,V,T)=\left(\frac{\partial F(N,V,T)}{\partial T}\right)_V. \tag{23}$$

In this way the effect of correlations on the entropy is included, since the temperature derivative involves also the finite temperature Brueckner contribution of Eq. (18).

C. Zero-temperature limit

It is instructive to look closely at the low temperature region of the present formalism. The independent particle part Ω_0' of the grand-canonical potential of Eq. (17) reduces, for $\beta\to+\infty$, to

$$\omega_0'\approx\frac{2}{\pi^2}\int k^2dk[(e_k-\mu)-U(k)n(k)]$$

$$\approx\frac{2}{\pi^2}\int k^2dk[t_k-\mu]=E_0-\mu\rho, \tag{24}$$

where t_k is the single-particle kinetic energy and E_0 the free particle ground state energy. Therefore, in this limit, ω_0' gives the free particle contribution. This result does not depend on the particular choice of the auxiliary potential U. This cancellation occurs also in the zero-temperature BBG formalism.

As mentioned above, the interacting part $\Delta\omega$ reduces to the Brueckner potential energy part in the low temperature limit, and therefore one gets

$$\omega \approx E_B - \mu\rho, \tag{25}$$

where E_B is the Brueckner ground state energy. Therefore, the free energy F coincides with E_B, as expected at zero temperature.

III. CORRECTIONS COMING FROM THREE-BODY FORCES

As is well known, the Brueckner approximation is unable to reproduce the correct phenomenological saturation point. Higher order terms in the hole-line expansion turn out to be much smaller, which indicates the convergence of the BBG expansion already at the two-hole-line level of approximation, provided the ''continuous'' choice for the single-particle potential is adopted. One has to assume that also three-body forces must be included in the nuclear Hamiltonian. Unfortunately, such forces, derived from first principles, are not yet available. The most complete study of three-body forces based on meson exchange theory is the one presented in Ref. [25], where most of the contributing processes were estimated, including phenomenological form factors, but still keeping consistency with two-body forces. Still large uncertainties are present, which lead many authors to introduce schematic three-body forces, with a structure suggested also by meson theory. The few parameters appearing in these forces are then adjusted in order to reproduce the correct saturation point and possibly the binding energy of the three-body nuclear systems. In particular the Urbana [26] interaction has such characteristics. It includes two terms, one attractive and the other repulsive,

$$V_{ijk} = V_{ijk}^{2\pi} + V_{ijk}^{R}. \tag{26}$$

The two-pion exchange contribution is a cyclic sum over the nucleon indices i, j, k of products of anticommutator and commutator terms,

$$V_{ijk}^{2\pi} = A \sum_{cyc} \Big(\{X_{ij}, X_{jk}\}\{\tau_i \cdot \tau_j, \tau_j \cdot \tau_k\} + \frac{1}{4}[X_{ij}, X_{jk}][\tau_i \cdot \tau_j, \tau_j \cdot \tau_k] \Big), \tag{27}$$

where

$$X_{ij} = Y(r_{ij})\sigma_i \cdot \sigma_j + T(r_{ij}) S_{ij} \tag{28}$$

is the one-pion exchange operator, σ and τ are the Pauli spin and isospin operators, and $S_{ij} = 3[(\sigma_i \cdot r_{ij})(\sigma_j \cdot r_{ij}) - \sigma_i \sigma_j]$ is the tensor operator. $Y(r)$ and $T(r)$ are the Yukawa and tensor functions, respectively, associated with the one-pion exchange interaction. The curled and square parentheses indicate the anticommutator and commutator, respectively. The summation is extended to the cyclic permutations of the three interacting particles. The repulsive part is taken as

$$V_{ijk}^{R} = U \sum_{\text{cyc}} T(r_{ij})^2 T(r_{jk})^2. \tag{29}$$

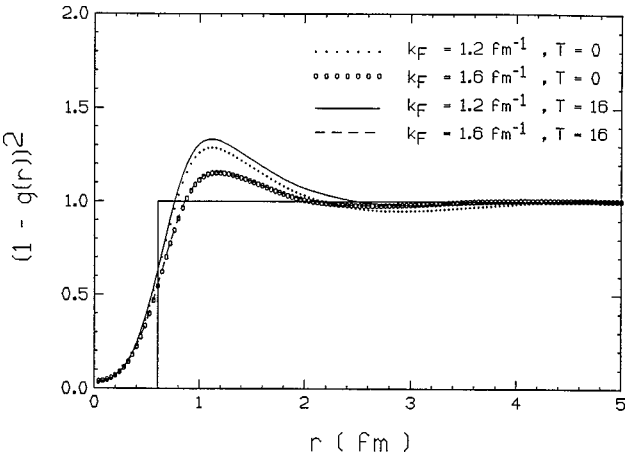

FIG. 5. Correlation function calculated at zero initial relative momentum in the $^1S_0$ channel for different densities and temperatures. The rectangular curve indicates the approximation used in calculating the three-body force of Eq. (C3) in Appendix C.

The strengths A (<0) and U (>0) can be fitted in order to reproduce the binding energy of triton and ^{3}He and the empirical nuclear matter parameters. It appears very difficult to fit simultaneously all these quantities, probably because three-body forces are in principle different for different systems. Therefore we prefer to adjust A and U to the nuclear matter saturation point only. Once these parameters are fixed, the whole nuclear matter EOS can be obtained. The values $A = -0.0329$ and $U = 0.00361$ have been found to give an accurate saturation point.

The method of including this interaction in the many-body scheme follows Ref. [27], where the three-body interaction is reduced to an effective two-body one, by an averaging over the third particle coordinates [23]. In this average the weight is given by the probabbility to have two particles at a certain distance r, that is, the two-body correlation function, which is reported in Fig. 5 for different densities and temperatures. The temperature dependence is quite weak and in the actual calculations it has been neglected. More details are given in Appendix C. The final form for the attractive part of Eq. (27) has the following structure:

$$v_3^{eff} = v_S(r_{ij})(\sigma_i \cdot \sigma_j) + v_T(r_{ij}) S_{ij}, \tag{30}$$

where the spin and tensor form factors v_S and v_T are simple integrals involving the functions Y and T, as explained in Appendix C. This effective force is added to the nuclear Hamiltonian H, and the calculations proceed along the same ordinary Brueckner scheme with only two-body forces, both at zero and finite temperature.

IV. THE EQUATION OF STATE AT FINITE TEMPERATURE

According to the formalism developed in the previous sections, to obtain the EOS at finite temperature one has to start solving Eqs. (9) and (12) self-consistently for the single-particle potential U at a fixed density and temperature. This implies that the chemical potential $\tilde{\mu}$ must be extracted at each step of the iterative procedure from Eq. (20). The procedure is quite analogous to the corresponding one at zero

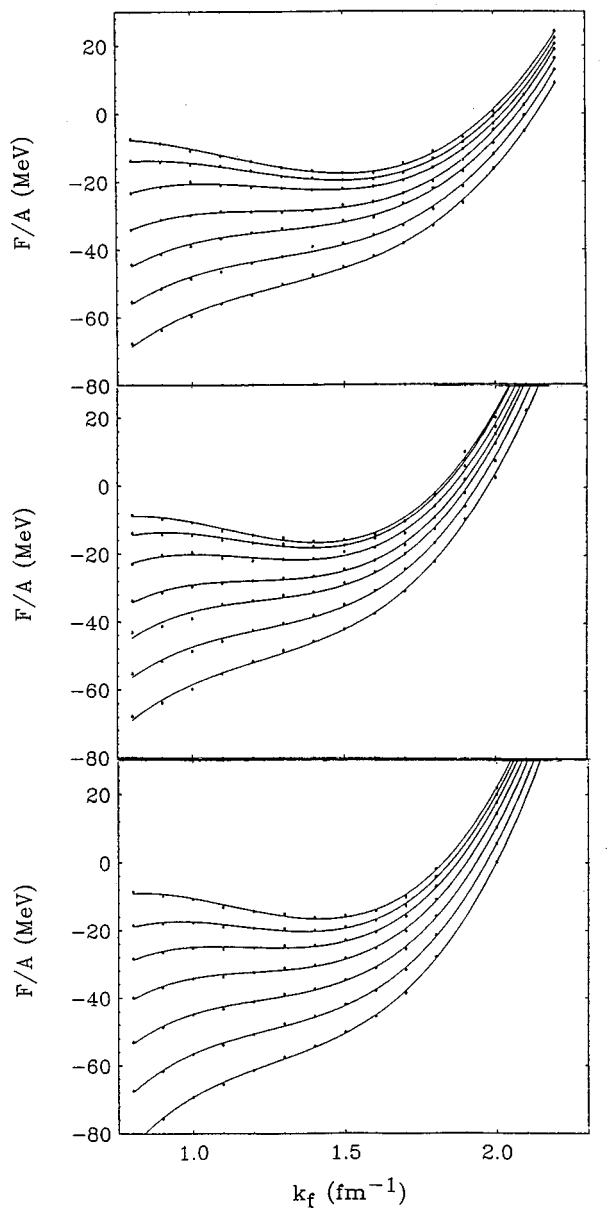

FIG. 6. Free energy of symmetric nuclear matter as a function of density and temperature. The dots represent the calculated values and the solid lines the spline fitting. The upper, middle, and lower figures report the results without 3BF's, with 3BF's, and for the free gas model. The free energy is a decreasing function of temperature and in each figure the upper curve corresponds to $T=0$ and the lower ones to temperatures of 8, 12, 16, 20, 24, 28 MeV.

temperature. Once the U potential and the K matrix are obtained, both unperturbed and interacting components Ω_0' and $\Delta\Omega$ of the grand-canonical potential Ω of Eq. (16) can be calculated, following Eqs. (17) and (18). As discussed in Appendix A, we prefer to separate the first term of the arctan expansion in Eq. (7), which gives the contribution ω_1, defined in Eq. (A11), to the grand-canonical potential. The contribution coming from all the other terms in the power expansion will be denoted by ω_h. The first term ω_1 is indeed the two-body correlation term, namely, the Brueckner approach, in the ''naive'' finite temperature BBG expansion introduced in Sec. II. The free energy is then calculated from Eq. (21), where $\tilde{\mu}$ is the chemical potential extracted from the density, as mentioned above.

TABLE I. Contributions (MeV) to the grand-canonical potential of the first term Ω_1 in the expansion of the arctan function of Eq. (7), in comparison with the higher order contribution Ω_h.

	$T=12$		$T=24$	
k_F	Ω_1	Ω_h	Ω_1	Ω_h
1.0	-22.822	0.311	-19.197	0.158
1.4	-39.213	0.403	-36.556	0.559
1.9	-36.411	0.652	-35.709	1.178

A. Symmetric nuclear matter

1. Critical temperature and critical density

Following this procedure, the results of the numerical evaluation of the free energy in symmetric nuclear matter with the Argonne v_{14} potential [28] as the bare NN interaction v are shown in Fig. 6, with and without the inclusion of three-body forces. The calculations were performed including all the channels up to $J=4$ and with a cutoff in momentum of the single-particle potential equal to $k_c=6$ fm^{-1}. The limitations in J and momentum are quite appropriate to the density region pertinent to the liquid-gas phase transition. In Fig. 6 the dots represent the calculated values and the solid lines a polynomial fit, essential for the numerical derivative needed to obtain the pressure $p=\rho^2\partial f/\partial\rho$ and the chemical potential μ of Eq. (B2). At $T=0$ the free energy coincides with the total energy and the corresponding curve is just the usual nuclear matter saturation curve. The relevance of three-body forces is immediately seen from the shift of the saturation point to $k_F\approx 1.4$ fm^{-1}, $e\approx -16$ MeV, close to the empirical one. The effect of these forces is also very small at low densities and becomes larger at increasing densities, where a much stronger repulsion is apparent. The steepness of the EOS at higher densities can depend of course on the particular three-body force introduced in the calculations, but the region around saturation is expected to be insensitive to the details of the force used, since they are constrained to reproduce this region. The critical point of the EOS should also be insensitive to the force since it occurs at very low density, of order of $\rho_0/3 - \rho_0/2$.

It is interesting to separate out the contribution ω_1 to the free energy coming from the first term of the power expansion of the arctan function of Eq. (7). This is done in Table I, for few characteristic temperatures and densities. As explained in Appendix B, the higher power terms in the expansion become vanishing small at low temperature. From Table I one can conclude anyhow that, in the temperature and density range we are interested in, the contributions ω_h of these higher order terms are at most a few percent of ω_1, and therefore they can be neglected still maintaining a good accuracy in the final result. This is equivalent to restricting the calculation within the naive finite temperature BBG expansion, the NTBBG scheme introduced in Sec. II. In this case the procedure we have followed to extract the free energy turns out to be strictly equivalent to the alternative procedure which involves the entropy expression of Eq. (22), as outlined at the end of Sec. II. Furthermore, for the same reason, the adopted definition of the single-particle potential of Eq. (12) differs very little from the choice advocated in the origi-

nal work of Bloch and De Dominicis [10]. This finding justifies the procedure often followed in the literature for finite temperature calculations in infinite nuclear matter [9] and in Hartree-Fock calculations for finite nuclei as well [29], where the temperature only enters through the finite temperature single-particle Fermi distributions.

The full knowledge of the temperature dependence of the free energy is only obtained after a complex numerical procedure. A hybrid free fermion gas model, often adopted [30], provides a simplified procedure to estimate this temperature dependence. In this schematic model one keeps fixed for all temperatures the total internal energy E of nuclear matter and equal to the one calculated at zero temperature for the full interacting model. The free energy $F=E-TS$ is then calculated by using for the entropy S the free Fermi gas, namely, the expression of Eq. (22) with the occupation number $n(k)$ derived from the free particle spectrum $\epsilon_k=t_k$ and the corresponding chemical potential extracted from Eq. (20). In other words, the effect of correlations on the entropy is neglected in the hybrid model. The results of this procedure are shown in Fig. 6, including three-body forces in E. The free energy appears to be systematically lower at all temperatures in comparison with the full microscopic calculation. As we will see, this is due to lower values of the entropy when the interaction is introduced, since then the effective mass m^* is smaller than the bare one, and in the low temperature region the entropy is proportional to the effective mass, $S/N=\pi^2T/E_F$, $E_F=\hbar k_F^2/2m^*$. The relevance of the comparison with the hybrid free fermion model, which keeps the correlations as frozen at zero temperature, is to show how significant is the temperature dependence of the correlations.

From the polynomial fit of the free energy it is easy to perform the numerical derivative that leads to the pressure $p=p(\rho,T)$. This is the most familiar form of the equation of state and is reported in Fig. 7 and in Tables II and III. For both cases, with and without three-body forces, the EOS displays the van der Waals behavior typical of a liquid system undergoing a liquid-gas phase transition. The trend of the chemical potential as a function of density and temperature has also the signature of the liquid-gas phase transition. In fact, from the relation

$$\rho\frac{\partial\mu}{\partial\rho}=\frac{\partial p}{\partial\rho}, \tag{31}$$

one can see that at the critical point the first and second derivatives of the pressure p are zero and so are the corresponding derivatives of μ. This is apparent in Fig. 8, where the chemical potential μ of Eq. (B2) is reported. The corresponding critical temperature can be traced from the isotherm which presents an inflection point at the critical density, both for the chemical potential and the pressure curves as a function of density. Numerically this can be achieved by performing a further derivative of the interpolated free energy of Fig. 6, identifying the isotherm which displays an inflection point. This, however, might not be sufficiently accurate. Therefore, we prefer to use an alternative method of looking at the phase transition, which requires only first order numerical derivatives, which is the specific cases of the chemical potential and pressure. It proceeds as follows. If one plots the chemical potential as a function of the pressure

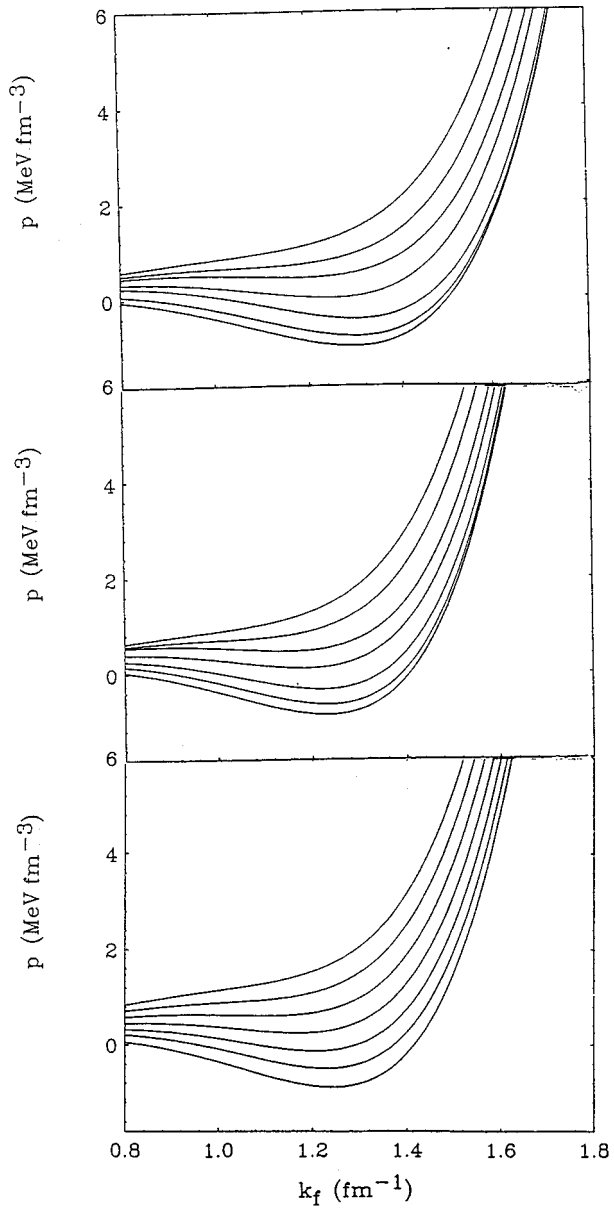

FIG. 7. The pressure as a function of density and temperature for symmetric nuclear matter. The upper, middle, and lower figures report the results without 3BF's, with 3BF's, and for the free gas model. The pressure increases with temperature and in each figure the isotherms correspond to $T=0$, 8, 12, 16, 20, 24, 28 MeV.

at different temperatures, as shown in Fig. 9, this plot should display the characteristic self-intersecting behavior, with three branches corresponding to the liquid, vapor, and unstable regions of the equation of state. The point of intersection, observed, for instance, in the lower part of Fig. 9 for the isotherm $T=20$ MeV, is the liquid-vapor coexistence point at that specific temperature, which disappears as the temperature increases above the critical one. However, our calculations do not touch the vapor region, occurring at very low densities; therefore the corresponding branch is absent, except for temperatures above 20 MeV. A complete representation would require quite lengthy numerical calculations in the low density region, which slowly converge and require a very fine grid in the momentum discretization of the equations. Anyhow, from our results it is possible to identify the critical point.

TABLE II. Pressure (MeV fm^{-3}) as a function of temperature (MeV) and Fermi momentum (fm^{-1}) without the inclusion of three-body forces.

				T			
k_F	0	8	12	16	20	24	28
0.8	-0.048	0.070	0.238	0.320	0.445	0.498	0.577
0.9	-0.189	-0.036	0.186	0.314	0.496	0.585	0.712
1.0	-0.397	-0.212	0.063	0.251	0.502	0.641	0.834
1.1	-0.650	-0.442	-0.122	0.143	0.473	0.679	0.959
1.2	-0.886	-0.670	-0.319	0.042	0.455	0.750	1.136
1.3	-0.995	-0.787	-0.425	0.051	0.548	0.952	1.464
1.4	-0.795	-0.614	-0.262	0.347	0.921	1.458	2.110
1.5	-0.013	0.122	0.443	1.206	1.838	2.532	3.331
1.6	1.732	1.814	2.088	3.023	3.682	4.554	5.496
1.7	4.961	4.994	5.222	6.342	6.982	8.051	9.116
1.8	10.353	10.366	10.574	11.890	12.448	13.724	14.866
1.9	18.782	18.836	19.088	20.605	20.994	22.480	23.626
2.0	31.341	31.548	31.961	33.675	33.787	35.471	36.507
2.1	49.370	49.914	50.678	52.576	52.275	54.127	54.891
2.2	74.540	75.659	77.057	79.115	78.232	80.203	80.472

The critical temperature T_c can then be identified at $T_c \approx 21$ MeV and $T_c \approx 20$ MeV in the calculation without and with the inclusion of three-body forces, respectively. It looks like the critical temperature T_c is not strongly affected by these forces.

The observation of the isotherms of Fig. 7 seems to suggest that the critical temperature, as defined by the occurrence of the inflection point in the pressure curve, is slightly larger than the values just quoted. As already mentioned, we prefer the criterion based on the self-intersection in the plot of the chemical potential versus the pressure, since it involves only first order derivatives.

It is more difficult to extract an accurate value for the critical density, from Fig. 7 or from Fig. 8. It can be estimated to be in the range between 0.068 and 0.09 fm^{-3}, both with and without three-body forces. These results confirm the main trend reported in Ref. [8] on the basis of the NTBBG, with a smaller number of two-body channels and

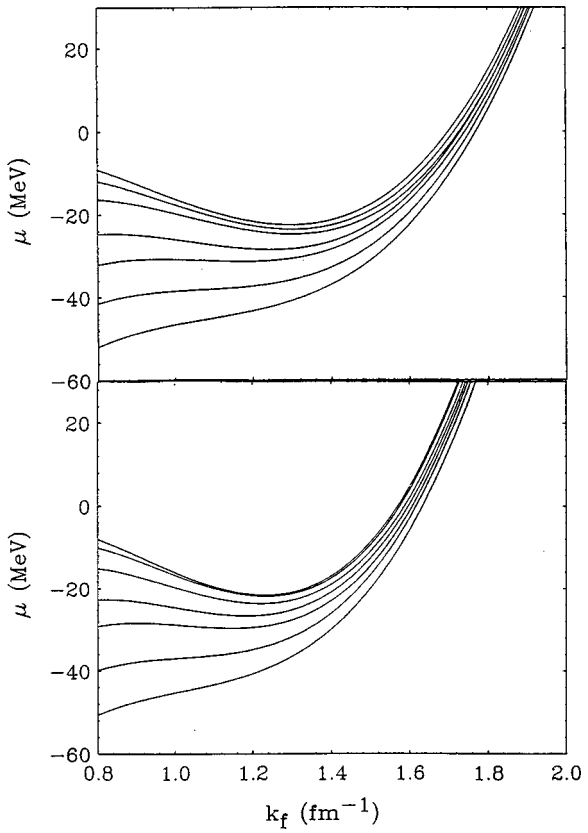

FIG. 8. Chemical potential for symmetric nuclear matter, as a function of density and temperature, calculated from Eq. (2) of Appendix B. The upper and lower figures correspond to calculations without and with 3BF's, respectively. μ decreases with temperature and in each figure is represented for the same temperatures of Fig. 6.

TABLE III. The same as in Table II with the inclusion of three-body forces.

				T			
k_F	0	8	12	16	20	24	28
0.8	0.028	0.149	0.259	0.396	0.536	0.567	0.630
0.9	-0.134	0.022	0.178	0.376	0.569	0.649	0.763
1.0	-0.373	-0.186	0.020	0.291	0.542	0.699	0.886
1.1	-0.643	-0.435	-0.177	0.176	0.487	0.753	1.039
1.2	-0.835	-0.620	-0.315	0.125	0.495	0.904	1.311
1.3	-0.753	-0.547	-0.206	0.319	0.743	1.321	1.867
1.4	-8.411	0.098	0.452	1.052	1.528	2.286	2.976
1.5	1.633	1.781	2.115	2.770	3.294	4.220	5.037
1.6	5.044	5.160	5.428	6.104	6.681	7.718	8.614
1.7	11.021	11.129	11.266	11.916	12.559	13.593	14.475
1.8	20.700	20.858	20.783	21.342	22.084	22.918	23.630
1.9	35.538	35.847	35.459	35.943	36.743	37.070	37.378
2.0	57.356	57.980	57.158	57.260	58.412	57.786	57.354
2.1	88.395	89.583	88.179	87.869	89.417	87.216	85.577
2.2	131.378	133.481	131.324	130.446	132.597	127.979	124.512

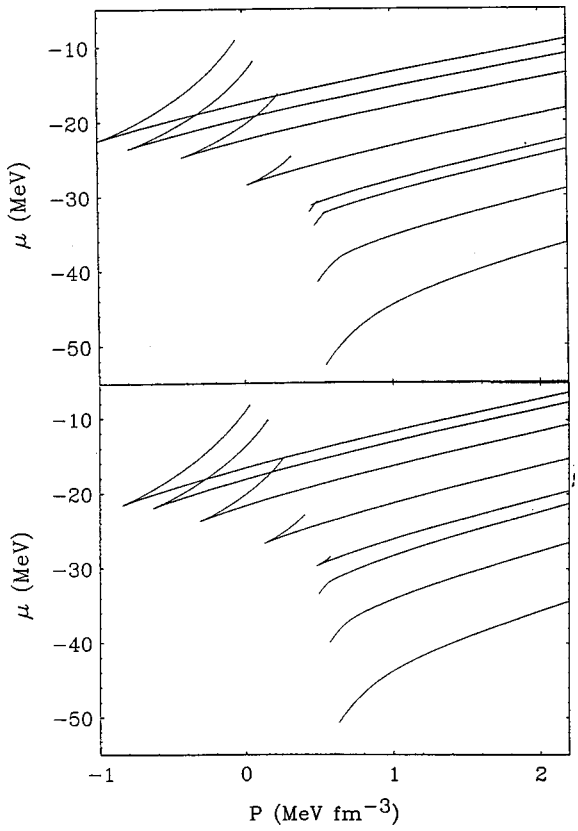

FIG. 9. The same as in Fig. 8 as a function of pressure. An additional temperature $T=21$ MeV in the critical region is considered and corresponds to the third curve from the bottom.

different cutoff parameters. The critical point is also close to the one calculated in Ref. [7] from a variational approach and a different interaction.

However, our results are quite different from the ones presented in Ref. [9], where a critical temperature $T_c \approx 9$ MeV was found. The authors restrict their calculations to above the critical temperature, since they claim to find numerical instabilities at lower temperatures. We did not find such a problem, and the iterative procedure turned out to be stable and to converge quite smoothly, as Fig. 6 certifies. This discrepancy is perhaps due to the use of a different interaction.

The van der Waals behavior was questioned in the finite temperature relativistic Dirac-Brueckner calculation of Ref. [31]. No critical point is apparent in the trend of the isotherms. These calculations were recently repeated [32] with a different interaction, the Bonn potential [33], and a liquid-gas phase transition was clearly observed at $T_c \approx 10$ MeV. It seems unlikely that such a lower critical temperature can be attributed to relativistic effects, since the critical density is a fraction of the saturation one, where relativistic effects are expected to play no role. The discrepancy surely deserves further studies.

The van der Waals behavior can be used to construct the liquid-vapor coexistent line by the standard Maxwell construction. However, the vapor region occurs at very low density, where the numerical solution of the self-consistent equations is difficult and requires a fine grid in momentum, as already mentioned.

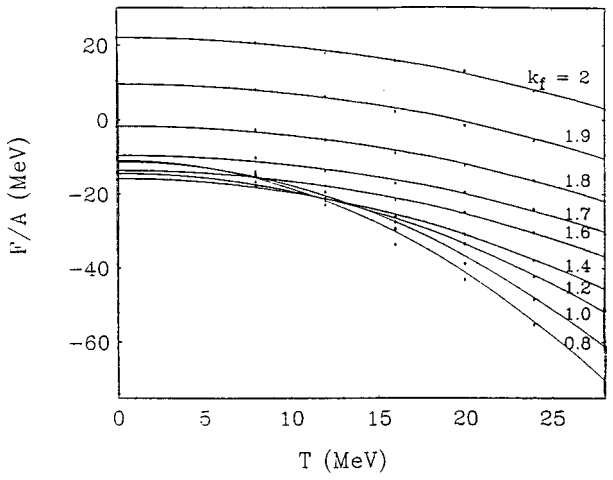

FIG. 10. Free energy of symmetric nuclear matter as a function of temperature at different densities with 3BF's. The dots represent the calculated values and the solid lines a quadratic fit.

2. Entropy and effective mass

The entropy is a thermodynamical quantity often discussed in connection with particle production in heavy ion collisions and in the determination of the isentropic evolution of supernova collapse. The entropy release in multifragmentation events is considered to be the crucial quantity to determine the fragment mass distribution [34]. In supernova collapse it is commonly believed that the evolution is isentropic, and therefore knowledge of entropy allows us to obtain the pressure as a function of ρ and S, that is, the relevant EOS.

As discussed at the end of Sec. II B, the entropy can be extracted from Eq. (23), once the free energy f is found as a function of temperature and density. In practice, we have found that F/A at a fixed density has a temperature dependence that follows closely a quadratic law, as shown in Fig. 10 in the calculation that includes 3BF's. The calculated values, indicated by points, lie on parabolic lines with sufficient accuracy. It is then straightforward to extract analytically the entropy, reported in Fig. 11, together with the entropy for a free Fermi gas. The comparison between the two seems to indicate a similar trend in the density dependence. However, the correlated system displays irregular regions for densities around $k_f=1.1$ and $k_f=1.7$ fm^{-1}, where a sudden change of slope is apparent. Furthermore, the temperature dependence seems to be more regular, as a consequence of the quadratic behavior of the correlated free energy. Both features can be traced back to the behavior of the effective mass as a function of temperature and density. The latter is calculated from the self-consistent single-particle potential $U(k)$, shown in Fig. 12, according to the relation

$$\frac{m^*(k)}{m}=\left[1+\frac{m}{\hbar^2 k}\frac{dU(k)}{k}\right]^{-1}. \tag{32}$$

The temperature dependence of U is weak in general, except at low density, where the depth of the potential at $k=0$ increases with temperature, as a consequence of the enlarged phase space available for the interacting particles. This is apparent from Eq. (9), where the Pauli operator $n_> \cdot n_>$ is

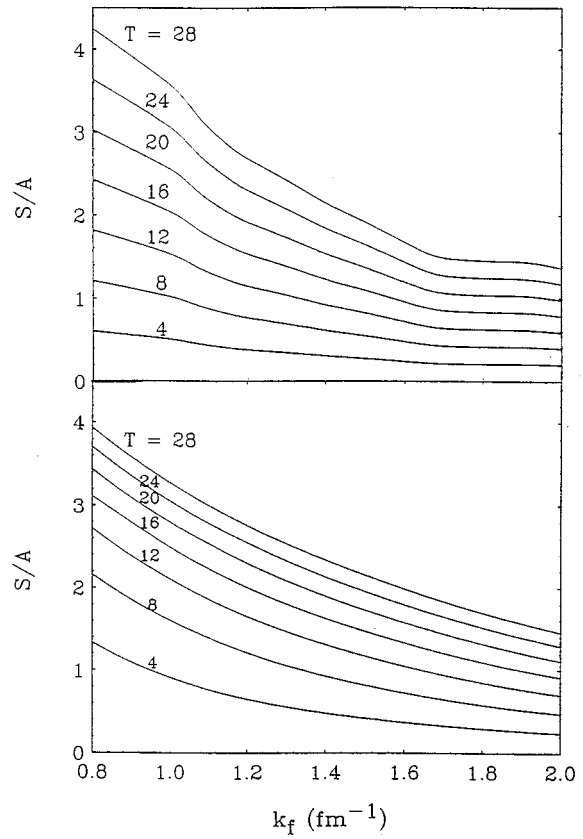

FIG. 11. Entropy of symmetric nuclear matter as a function of density at different temperatures. The lower figure corresponds to the free gas model and the upper one to the BD calculations with 3BF's.

smoothed with temperature, an effect which is stronger at smaller density, where T/E_F can be larger than 1. The sharp increase of U at large densities and high momenta is due to the presence of the 3BF's, which introduces a strong repulsion in this region. This behavior of U produces the drop of the effective mass in the same region, for example, at $k_F = 2$ fm^{-1}, shown in Fig. 13. The derivative in Eq. (32) was done with a five-point numerical differentiation. Similarly, the temperature dependence of the effective mass is quite weak, except at low densities, as one can see from Fig. 13. The effective mass at $T=0$ and $k_F=1.4$ has a value compatible with phenomenology related to the nuclear optical potential, which suggests $m^*/m \approx 0.7$ [18]. The temperature and density dependence of m^* at the Fermi momentum is reported in Fig. 14 for the same type of calculations. The effect of temperature brings a decrease in the effective mass, stronger at low densities. Consequently, the Fermi energy becomes substantially larger with respect to the free gas value. This can explain the already noticed smoother behavior of the entropy as a function of temperature, since then T/E_F is small enough for the linear dependence of the entropy on temperature to be valid. On the other hand, the density dependence of m^* at all temperatures shows a change in curvature, and can give an explanation of the change in slope observed in Fig. 11 for the correlated system. In particular, the fast increase of m^* at $k_F > 1.8$ is responsible for the corresponding change of slope in the density dependence of the entropy.

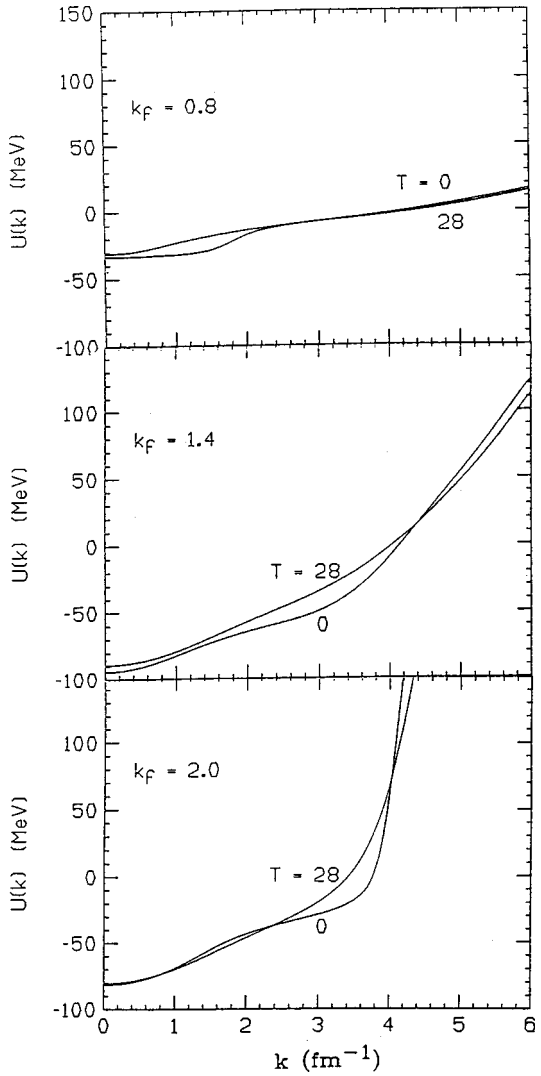

FIG. 12. The self-consistent single-particle potential of symmetric nuclear matter as a function of momenta at different densities and temperatures.

B. Neutron matter and supernova explosions

Analogous calculations were performed for pure neutron matter, with the inclusion of the same number of partial waves and the same momentum cutoff. As it is well known, neutron matter is unbound, as one can see in Fig. 15, where the free energy does not display a minimum at any temperature. As a consequence, the pressure, reported in Fig. 16, and in Table IV, is always positive and increases steeply at higher densities. This feature, together with the temperature dependence of the pressure, is important for the physics of supernova collapse, where, in the final bounce-off of the star, densities a few times larger than saturation and temperatures of few tens of MeV can be reached. The stiffness of the equation of state and the temperature dependence of the pressure are crucial elements in determining the final fate of the collapsing supernovas, which can finally end as a neutron star or a black hole or even fail to explode.

The EOS for neutron matter is much stiffer at high density when 3BF's are introduced. The stiffness is then comparable to the one obtained within the Dirac-Brueckner approach [35]. This is not surprising, since it is well known that rela-

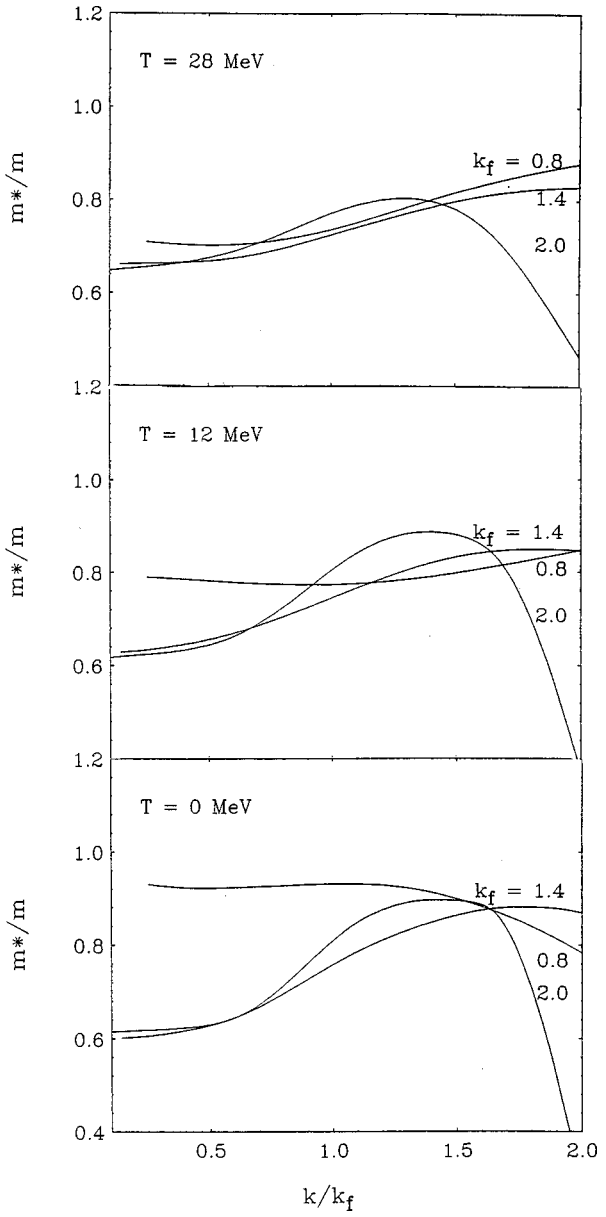

FIG. 13. Effective mass for symmetric nuclear matter as a function of momentum at different densities and temperatures.

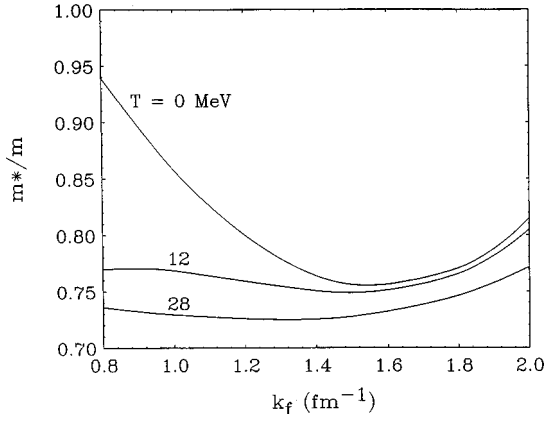

FIG. 14. Effective mass for symmetric nuclear matter at the Fermi surface as a function of density at different temperatures.

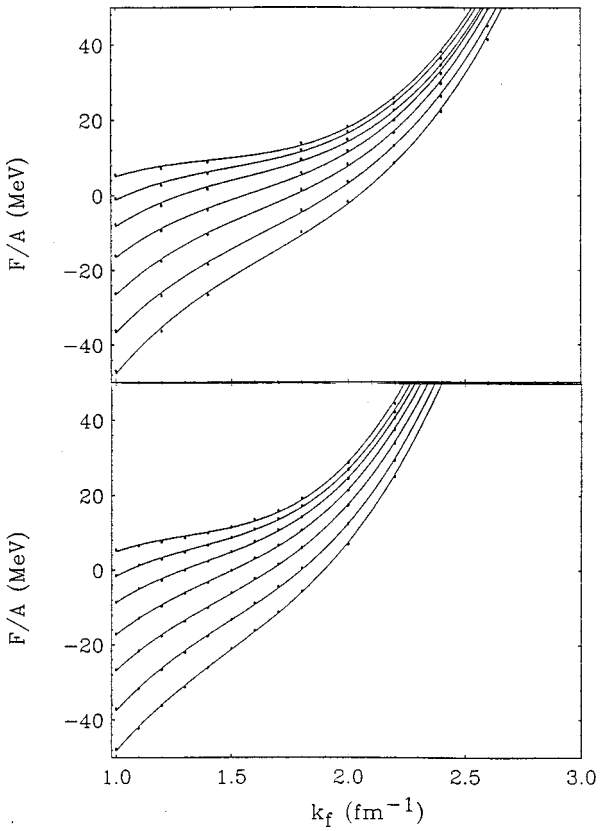

FIG. 15. Free energy of pure neutron matter as a function of density and temperature. The dots represent the calculated values and the solid lines the spline fitting. The upper and lower figures report the results without 3BF's and with 3BF's, respectively. The free energy is a decreasing function of temperature and in each figure the upper curve corresponds to $T=0$ and the lower ones to temperatures of 8, 12, 16, 20, 24, 28 MeV.

tivistic effects can be interpreted as a 3BF in the nonrelativistic reduction of the equations [36]. The EOS is also stiffer as the temperature increases, and certainly at temperatures of few tens of MeV this temperature effect cannot be neglected.

The collapse of a supernova involves actually asymmetric nuclear matter, which is kept out of β equilibrium with a large asymmetry, until the end of the neutrino trapping stage. During this period the asymmetry $a=(\rho_n-\rho_p)/(\rho_n+\rho_p)$ is expected to be between 0.2 and 0.4. Here ρ_n and ρ_p are the neutron and proton densities, respectively. It is therefore interesting to know the EOS of nuclear matter at different asymmetries. In previous studies of the EOS at zero temperature it has been found [37] that the energy per particle $e(a)$ has a simple quadratic dependence on the asymmetry,

$$e(a)\approx e(0)+[e(1)-e(0)]a^2. \tag{33}$$

Therefore, the EOS at zero temperature for any asymmetry is known from pure neutron matter, $a=1$, and symmetric nuclear matter, $a=0$. This is related to the validity of the so-called Lane equations [38], which establish the linear dependence of the depth of the single-particle potential on the asymmetry parameter at $T=0$. In fact, since the variation of Fermi momentum is approximately linear in asymmetry, the

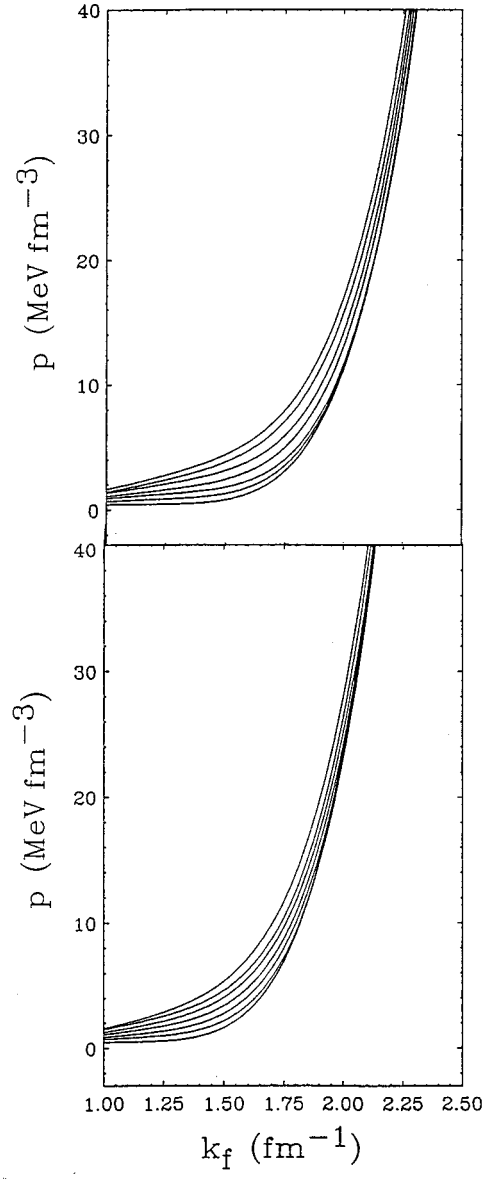

FIG. 16. The pressure as a function of density and temperature for pure neutron matter. The upper and lower figures report the results without 3BF's and with 3BF's, respectively. The pressure increases with temperature and in each figure the isotherms correspond to $T=0$, 8, 12, 16, 20, 24, 28 MeV.

energy of the proton and neutron components is approximately quadratic in a. This dependence turns out to be fulfilled to a large extent.

The single-particle potential is not strongly dependent on the temperature, at least for not too low densities, and the previous assumption should hold for $T\neq 0$. If we assume that this approximate quadratic behavior is valid also for the free energy at finite temperature, then from the neutron and symmetric nuclear matter EOS, discussed above, one can calculate the EOS at finite temperature for a generic asymmetry, according to an equation equivalent to Eq. (33) for the free energy. The resulting isotherms are shown in Fig. 17 for various asymmetries. The value $a=0.33$ is expected to be typical of supernova collapse. The liquid-gas phase transition disappears for some critical value of the asymmetry. The trend of the critical temperature as a function of asymmetry is most easily found by observing the behavior of the chemical potential as a function of pressure. Following this procedure the phase transition turns out to disappear at an asymmetry of approximately 0.9, as shown in Fig. 18. This result is in agreement with the Dirac-Brueckner calculation of Ref. [32]. It has to be noticed that T_c remains pretty constant up to an asymmetry as large as 0.4, which encompasses $a\approx 0.33$, the range of asymmetry typical of supernova explosion [39].

The EOS at finite temperature can be characterized by the value of the incompressibility K. In a thermodynamical context K is usually defined by $K=\rho\, dp/d\rho$, which explicitly identifies the spinodal region of the EOS as the one characterized by $K<0$. The standard nuclear physics definition at saturation is instead $K=k_F^2\, d^2F/dk_F^2$. In order to reconcile these two definitions we adopt here the thermodynamical one normalized in order to agree with the nuclear physics definition at saturation, namely,

$$K=9\frac{dp}{d\rho}. \tag{34}$$

It has been claimed [40] that, in order to have a successful supernova explosion in model simulations, the value of the incompressibility for symmetric nuclear matter at saturation must be not larger than approximately 100 MeV, a value much smaller than the one extracted from the frequency of the monopole excitation in nuclei. More recently [41] this conclusion was questioned on the basis of the ''neutrino revival'' model [42]. One has to stress, anyhow, that it is essential to take into account the dependence of the incompressibility on density, asymmetry, and temperature before drawing any conclusions. The incompressibility reported in Fig. 19 shows a very weak dependence on temperature at high densities, $\rho>\rho_0$, typical of the bounce-off stage in the supernova collapse. For symmetric nuclear matter, at saturation and zero temperature $K\approx 200$ MeV. It has to be noticed that in the bounce-off stage of the collapse temperatures of several tens of MeV are expected to be reached, and therefore the proper temperature dependence of the incompressibility should be included. A steep increase of K is observed as the density becomes higher, and the change of slope for $\rho>0.25$ was found to be related to the presence of 3BF's. The range of variation of K is quite similar to the one obtained in the Dirac-Brueckner approach [35]. The dependence on asymmetry also appears to be strong.

Figure 19 also shows that $T=24$ is above T_c, the value of K is always positive, and the liquid phase does not exist any more. From this figure it is also possible to identify the critical temperature for a certain asymmetric matter. For example, at $a=0.75$ the critical temperature is approximately 12 MeV and $\rho_c\approx 0.07$ fm^{-3}, the point where the incompressibility has a minimum and equals zero. At $T=0$ it seems possible to produce stable matter with an asymmetry very close to 1, that is, a neutron superrich matter, where a sort of neutron ''drip line'' for an infinite system is located.

V. LIMITING TEMPERATURE OF FINITE NUCLEI

The liquid-gas phase transition of nuclear matter, if it exists, does not possess a direct correspondence in finite nuclei,

TABLE IV. The same as in Table III for pure neutron matter.

				T			
k_F	0	8	12	16	20	24	28
1.0	0.544	0.836	1.028	1.237	1.419	1.603	1.745
1.1	0.559	0.917	1.172	1.452	1.705	1.959	2.165
1.2	0.574	0.990	1.315	1.675	2.012	2.350	2.637
1.3	0.653	1.109	1.508	1.955	2.388	2.811	3.211
1.4	0.911	1.381	1.854	2.391	2.930	3.467	3.979
1.5	1.534	1.980	2.521	3.144	3.793	4.438	5.095
1.6	2.790	3.165	3.762	4.461	5.217	5.967	6.791
1.7	5.058	5.305	5.937	6.693	7.543	8.384	9.398
1.8	8.844	8.898	9.534	10.318	11.238	12.144	13.368
1.9	14.809	14.600	15.200	15.970	16.917	17.848	19.297
2.0	23.795	23.253	23.763	24.461	25.375	26.269	27.956
2.1	36.857	35.913	36.265	36.821	37.614	38.386	40.315
2.2	55.288	53.884	53.995	54.315	54.873	55.409	57.575
2.3	80.654	78.749	78.519	78.494	78.665	78.819	81.203
2.4	114.833	112.414	111.723	111.218	110.811	110.396	112.968

due to the presence of Coulomb and finite size effects. In particular, the Coulomb interaction is of long range and strong enough to modify the nature of the phase transition. It has been recognized by several authors [43,44], however, that the nuclear EOS is related to the maximal temperature a nucleus can sustain before reaching mechanical instability. This ''limiting temperature'' T_l is mainly the maximal temperature at which a compound nucleus can be observed. The difficulty in observing a temperature up to T_l in such a system can be due not only to mechanical instability but also to

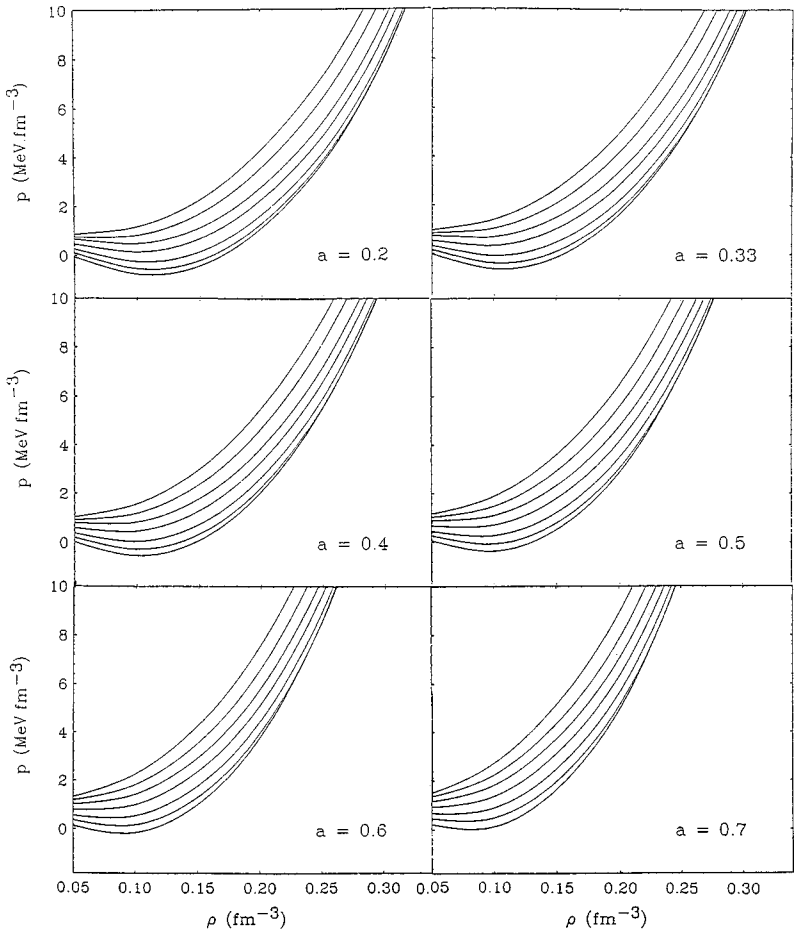

FIG. 17. The pressure as a function of density and temperature at different asymmetry a. All the calculations include 3BF's. The pressure increases with temperature and in each figure the isotherms correspond to $T=0$, 8, 12, 16, 20, 24, 28 MeV.

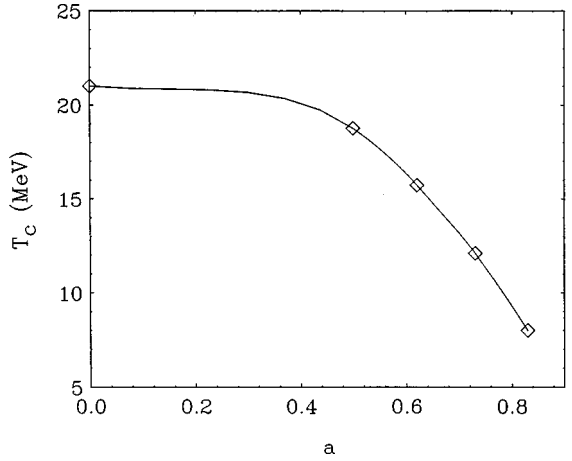

FIG. 18. Critical temperature of the nuclear liquid-gas phase transition as a function of asymmetry a. The squares correspond to the calculated points.

dynamical limitations in the reaction leading to compound nucleus formation. Anyhow, the limiting temperature is surely an upper limit for the maximal temperature observed experimentally. Fusion reactions between heavy ions at intermediate energies are an ideal tool for studying hot nuclei [46]. From the fit, by means of the statistical model, of the gamma ray and particle spectra, the presence of the compound nucleus and the value of its temperature was inferred in several fusion reactions.

Within this framework it is therefore interesting to extract from our microscopic EOS the corresponding limiting temperature. The connection between nuclear matter and finite nuclei requires the inclusion of Coulomb and surface tension corrections. Following Ref. [43] both corrections can be evaluated within the liquid drop model, which should be accurate enough for medium-heavy nuclei. The nucleus is described in terms of a droplet surrounded by a vapor, in thermal and mechanical equilibrium. This is equivalent to adding to the droplet pressure and chemical potential the contributions due to the Coulomb force and surface tension, which are evaluated assuming a spherical droplet. These additional terms read

$$\delta P = P_C + P_S = \left(\frac{Z^2 e^2}{5A} \rho - 2\alpha(T) \right) \Big/ R,$$

$$\delta \mu = \frac{6 Z^2 e^2}{5AR}, \tag{35}$$

where R is the droplet radius $R=(3A/4\pi\rho)^{1/3}$, ρ is the droplet density, and for $\alpha(T)=\alpha_0(1+\frac{3}{2}T/T_c)(1-T/T_c)^{3/2}$, with $T_c=20$ MeV, the nuclear matter critical temperature, and the surface tension at zero temperature, $\alpha_0 = 1.14$ MeV fm^{-2}, obtained from the semiempirical mass formula. The Coulomb interaction introduces an additional positive pressure P_C and a repulsive contribution to the bulk chemical potential μ, while the surface tension provides an additional negative pressure term which tends to stabilize the system. At increasing temperature the surface tension decreases and the system becomes unstable against Coulomb dissociation. The simplest way to observe the modifications

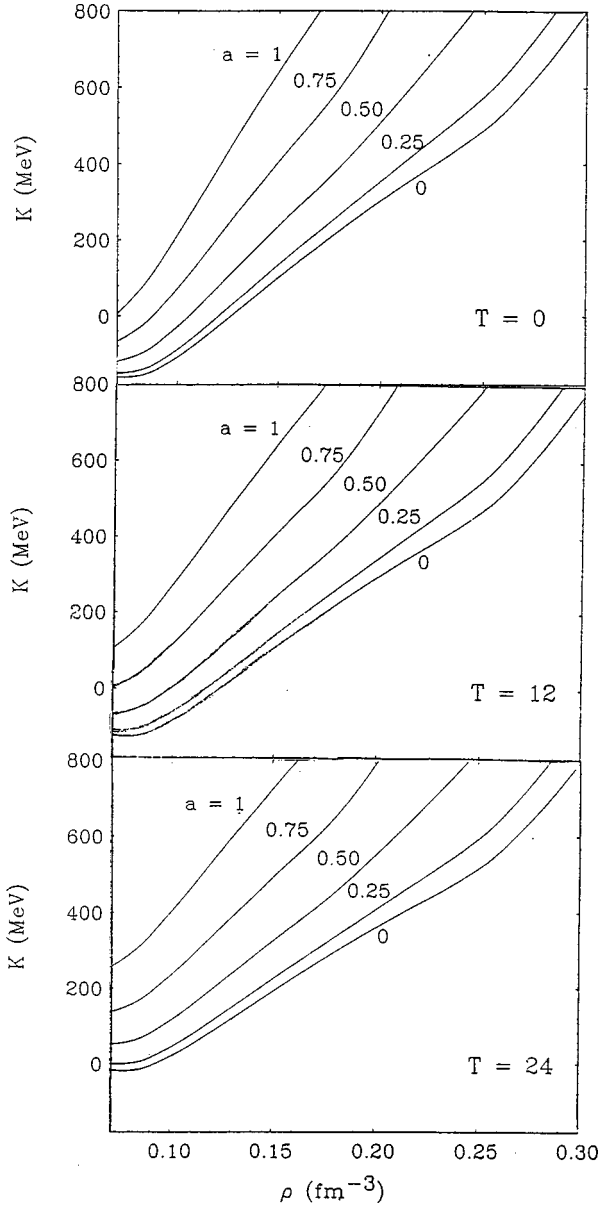

FIG. 19. Incompressibility parameter as a function of density for different values of the asymmetry a and different temperatures.

introduced by these terms is to consider the plot of the chemical potential as a function of pressure of Fig. 9 for nuclear matter. As previously explained, the intersection between the liquid and the vapor branches defines the coexistence point in nuclear matter. The additional terms will only shift the liquid branch, since the vapor is assumed to be uniform and uncharged, leading to a new coexistence point. Unfortunately, as already mentioned, it is very difficult to extend our microscopic calculations in the vapor region at the low temperatures needed for this estimation. In order to overcome this difficulty we have assumed that the single-particle self-consistent potential $U(k)$ tends to zero linearly with density. This assumption can be justified by noticing that the expression for the single-particle potential involves an integration over one hole line, according to Eq. (12). If one neglects the momentum dependence of the K matrix, one indeed obtains a density factor. We have therefore taken the self-consistent potential, calculated with 3BF's at the lowest

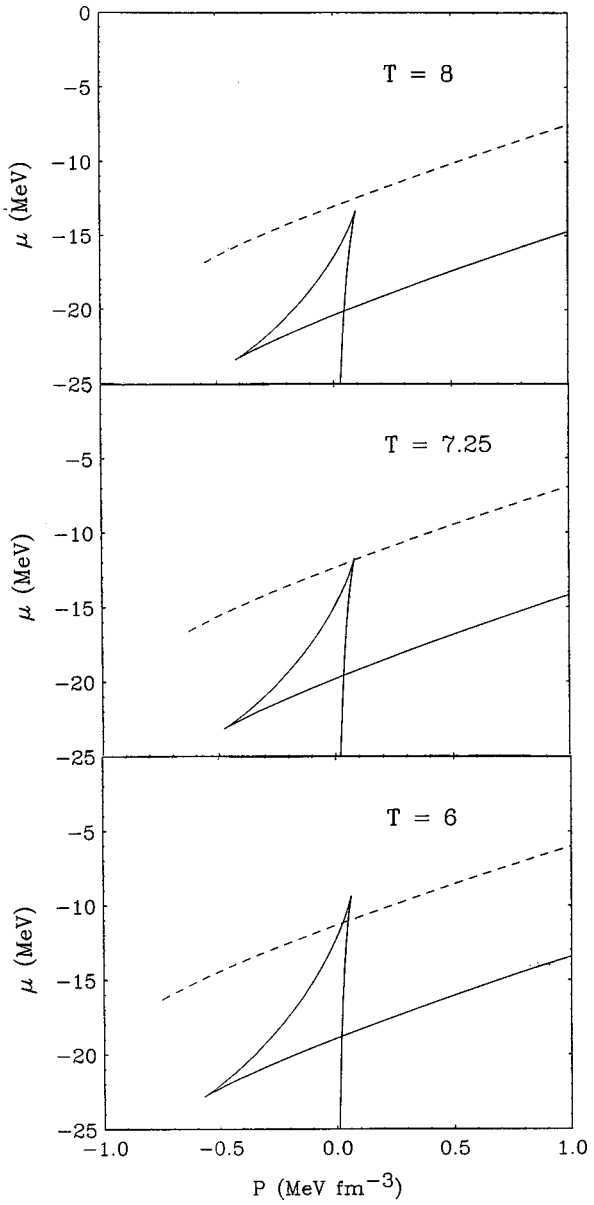

FIG. 20. Chemical potential for symmetric nuclear matter, with 3BF's as a function of pressure at different temperatures (solid line), calculated from Eq. (B2) of Appendix B, with the extrapolation to low densities of the single-particle potential, discussed in Sec. V. The dashed line corresponds to a liquid droplet of the nucleus Ag. The intersection between the two lines at $T=7.25$ defines the limiting temperature.

Fermi momentum $k_F=0.8$ fm^{-1}, U_0, and assumed that at lower density it has the form $U(k)=U_0(k)(k_F/0.8)^3$. Since the temperature dependence of $U(k)$ is very weak, as one sees in Fig. 12, at least for the low temperature relevant here, we kept fixed the potential with temperature. Once the single-particle potential is known, the EOS at low densities can be readily extracted from Eqs. (16) and (18), which depends only on $U(k)$, if one neglects ω_h in the arctan expansion. These higher order contributions are indeed negligible, as discussed in Sec. IV. The vapor, which occurs at very low densities, is then naturally included, as shown in the μ-P plots of Fig. 20, corresponding to the almost vertical branch, which intersects the liquid branch at the nuclear matter coexistence point. Including the corrections of Eq. (35),

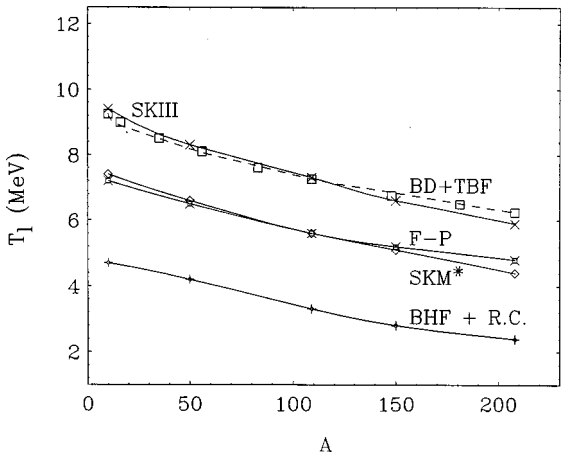

FIG. 21. Limiting temperature of finite nuclei, as a function of the mass number A, along the stability line. The squares correspond to the present BD finite temperature calculation with 3BF's. The curves SKIII and SKM* refer to the Skyrme force calculations of Ref. [43], F−P to the variational approach of Ref. [7], and BHF+RC to the Brueckner-Hartree-Fock with relativistic corrections of Ref. [45].

for the case of the Ag nucleus, the new liquid branch, indicated by the dashed lines, shows a shift with respect to nuclear matter. At low enough temperature an intersection between the liquid and vapor branches still occurs, which corresponds to the coexistence point between the liquid droplet and the nuclear matter vapor and assures that the droplet is stable. Increasing the temperature, the curve for nuclear matter shrinks and should collapse to a point at T_c. Before T_c it is possible to find a limiting temperature for which the intersection between the liquid droplet and the vapor branches is still possible. This determines T_l, which, in the case of Ag, is equal to 7.25 MeV.

The presence of the vapor phase is obviously a necessary ingredient of the model to assure thermodynamical equilibrium, and it is absent in reality. The effect of the vapor is essentially an additional stabilizing pressure, and therefore T_l can be again considered an upper limit for the reachable temperature.

The droplet-vapor coexistent point and, consequently, T_l depend on the mass and charge of the system. This dependence is studied in Fig. 21, where T_l is reported along the nuclear stability line, and compared with other EOS, taken from Ref. [45]. The results coming from the present calculations show a close agreement with the ones obtained from the phenomenological Skyrme force model SKIII of Ref. [44]. A strong dependence on EOS is anyhow observed. In particular, the Brueckner-Hartree-Fock calculations with relativistic corrections [45], which gives an EOS close to the Dirac-Brueckner one, display a very low T_l. This is not surprising, since also the critical temperature T_c is very low, approximately 9 MeV, as previously mentioned.

Although the connection between T_l and the nuclear EOS is not straightforward, the observation of a compound nucleus with a temperature larger than T_l would rule out the corresponding EOS. Compound nuclei with mass $A\approx 115$ with a temperature up to $T=6-7$ MeV have recently been observed [46]. This seems to put strong constraints on the possible nuclear matter EOS, as can be seen from Fig. 21.

VI. CONCLUSIONS

In the present work we have applied the finite temperature linked diagrammatic expansion developed by Bloch and De Dominicis to the study of the equation of state of nuclear and neutron matter. The reason for the choice of this formalism comes from the possible comparison one can make with the Bethe-Brueckner-Goldstone expansion in the zero-temperature limit. At the two-body correlation level the BD formalism contains terms which correspond to the Brueckner approximation, where the single-particle occupation numbers n are replaced by the finite temperature Fermi distributions. This selection of diagrams is also possible for three or higher order correlation diagrams. In the text we named these terms the ''naive'' temperature-dependent BBG expansion. The remaining finite temperature diagrams vanish in the zero-temperature limit and originate from the fact that at finite temperature any momentum state can be interpretated both as a particle and as a hole, and therefore they contain factors of the form $n(1-n)$. We found that at the two-body correlation level these additional diagrams are very small, at least in the range of temperatures relevant for the liquid-gas phase transitions, that is, below 30 MeV, and can be neglected in first approximation. At zero temperature the Brueckner two-hole-line approximation within the ''continuous'' choice includes most of the higher order correlations. The conclusion about the dominance of the diagrams contained in the NTBBG expansion suggested that the accuracy of the two-body approximation is still valid at finite temperature, using the ''continuous'' choice for the single-particle potential. According to the previous statement, our calculations include only two-body correlations and are dominated by the NTBBG terms. The self-consistent equations involve both the single-particle potential and the chemical potential, and are solved numerically by means of an iterative procedure, in order to obtain the grand-canonical potential and consequently the free energy.

The calculation of the different thermodynamical quantities can introduce some inconsistencies, related to the scheme of approximation, which can be summarized by the violation of the Hughenholtz–Van Hove theorem. We have suggested a procedure to extract the pressure and the chemical potential, both from the calculated free energy, which automatically fulfill the theorem.

For the nucleon-nucleon interaction we choose the Argonne v_{14} potential. Since three-body forces are required to have an EOS consistent with the semiempirical saturation point, we have included a phenomenological three-body force, which has been reduced to an effective two-body one and adjusted to reproduce the correct saturation point.

The finite temperature equation of state for symmetric nuclear matter displays a clear van der Waals pattern of behavior in the pressure-density plane, indicating the presence of a liquid-gas phase transition. With the three-body force included, the critical temperature turns out to be $T_c \approx 20$ MeV and $T_c \approx 21$ MeV with two-body force only. This value is consistent with Ref. [7], but is quite different from the one of Ref. [9] of $T_c \approx 9$ MeV, probably due to the use of a different interaction. The critical density ρ_c is found to be in the range between 0.068 and 0.09 fm^{-3} both with and without three-body force. The uncertainity in this result is due to the difficulty in identifing precisely the inflection point along an isotherm. This value of the critical density appears, anyhow, to be substantially larger than the one commonly found with Skyrme forces, around one-third the saturation density, that is, ~ 0.05 fm^{-3}.

The entropy, as a function of density and temperature, has a range of values similar to the ones calculated from the free gas model. However, the trend for the correlated system is strongly affected by the variation of the effective mass with density and temperature. This is a consequence of the behavior of the single-particle potential, which depends strongly on density and very little on temperature, but with a smoother momentum dependence at higher temperatures. At low temperature $m^*/m \approx 0.7$ at saturation, compatible with phenomenology.

For neutron matter no phase transition is present, since the system is unbound. From symmetric nuclear matter and neutron matter we have extracted the equation of state for a generic value of the asymmetry a by assuming a quadratic dependence of the free energy on a, consistent with Ref. [37]. The phase transitions seem to disappear only at a very large value of the asymmetry, $a \approx 0.9$, in agreement with similar relativistic Dirac-Brueckner calculations [32]. However, the value of the critical temperature in recent DB calculations is much smaller, $T_c \approx 10$ MeV. At zero temperature asymmetric matter becomes a bound system by a slight decrease of the asymmetry from $a=1$, and therefore the ''drip line'' for nuclear matter occurs at very large asymmetry.

The incompressibilty at saturation is about $K \approx 200$ MeV, a value strongly increasing with asymmetry and with temperature, at least at the high densities and temperatures relevant for supernova explosions.

For finite nuclei it is not possible to define a critical temperature. The concept of ''limiting temperature'' has been introduced instead, as the maximum temperature a nucleus can sustain before decaying [43]. The value of this temperature can be considered as an upper limit of the maximum temperature observed experimentally for a compound nucleus. This theoretically defined limiting temperature T_l can be extracted from the EOS of nuclear matter by including Coulomb and finite size effects. We have studied T_l along the nuclear stability line, assuming that Coulomb forces and surface tension are the ones of a spherical droplet [43], and compared with other EOS. The values obtained for T_l follow the trend obtained with the EOS extracted from the Skyrme force SKIII [44], and are larger than the ones predicted by all the available calculations. It has to be noticed that the experimental observation of a compound nucleus with a temperature larger than the value of T_l would necessarily rule out the corresponding EOS. There is experimental evidence that compound nuclei in the $A=115$ mass region can be produced up to 6–7 MeV [46] of temperature. Our equation of state is consistent with such findings, a fact not guaranteed by other EOS.

In conclusion, we have calculated within an accurate theoretical model the microsopic EOS with a realistic NN interaction and with inclusion of three-body forces. The EOS has the correct saturation point, predicts the critical temperature for the liquid-gas phase transitions, not yet so well established in the literature, and allows one to extract a limiting

temperature for finite nuclei consistent with the available phenomenology on compound nucleus formation in heavy ion reactions.

Finally, we would like to stress that the usual approach to finite temperature calculations, especially in finite nuclei, of introducing the temperature only through the smearing of the Fermi surface by means of a Fermi distribution, was found to be justified.

APPENDIX A

In this appendix we develop the explicit analytical form of the grand-canonical potential used in the numerical calculations. Let us start from Eq. (7) and define the operator $A(\omega)=B(\omega)\delta(H_0'-\omega)$, with $B(\omega)=\pi\mathcal{K}(\omega)$. The matrix element of this operator in the two-particle state basis can be written then as

$$\langle k_1k_2|A(\omega)|k_3k_4\rangle=\left(\frac{(2\pi)^{3/2}}{\sqrt{V}}\right)^4\delta(\mathbf{k}_1+\mathbf{k}_2-\mathbf{k}_3-\mathbf{k}_4)\,\delta(e_{k_3}+e_{k_4}-\omega)[k_1k_2|B(\omega)|k_3k_4]$$

$$=\langle qP|A(\omega)|q'P'\rangle=\left(\frac{(2\pi)^{3/2}}{\sqrt{V}}\right)^4\delta(\mathbf{P}-\mathbf{P}')\,\delta(E_{\mathbf{q}'\mathbf{P}'}-\omega)[q|B(\omega,\mathbf{P})|q'], \tag{A1}$$

where we have changed from the discrete momenta representation to the continuous one, denoted by the parentheses. The factors correspond to the conservation of total momentum and to the explicit δ function appearing in the operator A. In the second step we have introduced the relative momentum $\mathbf{q}=(\mathbf{k}_1-\mathbf{k}_2)/2$ and the total momentum $\mathbf{P}=\mathbf{k}_1+\mathbf{k}_2$ of the two particles, and the state $|q)$ is specified by the momentum $\mathbf{q}$ as well as by the corresponding spin-isospin quantum numbers $\sigma\,\tau$. The quantity E_{qP} corresponds to the two-particle energy in terms of the relative and total momenta,

$$E_{\mathbf{qP}}=\frac{\hbar^2\mathbf{q}^2}{m}+\frac{\hbar^2\mathbf{P}^2}{4m}+U\left(\left|\mathbf{q}+\frac{1}{2}\mathbf{P}\right|\right)+U\left(\left|\mathbf{q}-\frac{1}{2}\mathbf{P}\right|\right). \tag{A2}$$

If we now expand the arctan function,

$$\arctan(A)=\sum_n a_nA^n,\quad a_n=\frac{(-1)^{n-1}}{n},\quad n=\text{odd}, \tag{A3}$$

the expression of Eq. (7) for the grand-canonical potential can be written explicitly as

$$\Omega-\Omega_0'=\frac{1}{2}\int_{-\infty}^{+\infty}\frac{e^{-\beta\omega}}{\pi}\sum_n a_n\left(\frac{V}{(2\pi)^3}\right)^2\int d^qd^3P\left(\frac{V}{(2\pi)^3}\right)^2\int d_1^qd^3P_1[qP|A(\omega)|q_1P_1]$$

$$\times\left(\frac{V}{(2\pi)^3}\right)^2\int d_2^qd^3P_2[q_1P_1|A(\omega)|q_2P_2]$$

$$\times\cdots\left(\frac{V}{(2\pi)^3}\right)^2\int d_{n-1}^qd^3P_{n-1}[q_{n-2}P_{n-2}|A(\omega)|q_{n-1}P_{n-1}][q_{n-1}P_{n-1}|A(\omega)|qP]. \tag{A4}$$

Using the conservation of total momentum $\delta(\mathbf{P}-\mathbf{P}_j)$ in each matrix element of A, all the total momenta integrations can be performed, with exception of the one pertaining to the trace. Similarly the ω integration can be trivially done using one of the energy conservation functions $\delta(E_{\mathbf{qP}}-\omega)$ as defined in Eq. (8); one gets

$$\Omega-\Omega_0'=\frac{1}{2}\delta(0)\sum_n a_n\int d^3qd^3P\frac{e^{-\beta E_{\mathbf{qP}}}}{\pi}\int d^3q_1[q|B(E_{\mathbf{qP}},\mathbf{P})|q_1]\delta(E_{\mathbf{qP}}-E_{\mathbf{q}_1\mathbf{P}})$$

$$\times\int d^3q_2[q_1|B(E_{\mathbf{qP}},\mathbf{P})|q_2]\delta(E_{\mathbf{qP}}-E_{\mathbf{q}_2\mathbf{P}})\cdots[q_{n-1}|B(E_{\mathbf{qP}},\mathbf{P})|q]. \tag{A5}$$

The previous equations are exact at the two-body correlation level. As in standard Brueckner calculations, one approximates the Pauli operator $Q(\mathbf{q},\mathbf{P})=n_>(|\mathbf{q}+\frac{1}{2}\mathbf{P}|)n_>(|\mathbf{q}-\frac{1}{2}\mathbf{P}|)$ in Eq. (9) for the matrix K by its angular average,

$$\overline{Q}(q,P)=\frac{1}{4\pi}\int d\Omega_{qP}Q(\mathbf{q},\mathbf{P}). \tag{A6}$$

In this way the K matrix is diagonal in the two-body channel representation $lSJT$. This approximation turns out to be quite accurate [47]. Similarly, the matrix $\mathcal{K}$, and therefore B, can become diagonal if we also average the Pauli operator appearing in the defining equation (8). In Eq. (A5) the channels are still coupled, due to the angle dependence of the two-particle energies $E_{\mathbf{qP}}$, according to Eq. (A2). We there-

fore introduce a similar angle average approximation $\overline{E}_{qP}$ for these energies. Within these approximations the δ functions appearing in Eq. (A5) can be written as

$$\delta(\overline{E}_{qP}-\overline{E}_{q'P'})=\delta(q-q')/d(q,P), \tag{A7}$$

where the quantity $d(q,P)$ is defined in Eq. (19). Equation (A7) holds true if the energies $\overline{E}_{qP}$ are monotonic functions of q for a given value of P, which is usually the case in all practical applications. The expansion in partial waves of each B factor in Eq. (A5) is now straightforward. After integration over the angle of each momenta $\mathbf{q}_i$, all the matrix elements $(q|B|q)$ are diagonal in the channel quantum numbers and all equal to each other. This leads to

$$\Delta\Omega=\frac{1}{2}\frac{V}{(2\pi)^3}\sum_{lSJT}\hat{J}^2\hat{T}^2\int dq\int d^3P\frac{e^{-\beta(\overline{E}_{Pq}-2\mu)}}{\pi}\times d(q,P)\sum_n a_n\left[\frac{\pi[ql|K^{SJT}(\overline{E}_{Pq})|ql]q^2\overline{Q}(q,P)}{d(q,P)}\right]^n. \tag{A8}$$

We can now sum up the power expansion again, and get Eq. (18) for the grand-canonical potential.

In standard zero-temperature Brueckner calculations the angular average over the entry energy $E(\mathbf{P},\mathbf{q})$ is not necessary, since the angular integration can be done explicitly. For sake of comparison with the zero-temperature limit, we have separated out the first term in the power expansion of the inverse tangent, which has the same form as the zero-temperature Brueckner expression for the potential energy, with the occupation numbers given by the temperature-dependent Fermi functions. Taking the term with $n=1$ in Eq. (A5), one gets

$$\Omega-\Omega_0'=\frac{1}{2}\delta(0)\int d^3qd^3Pe^{-\beta E_{\mathbf{qP}}}[q|K(E_{\mathbf{qP}},\mathbf{P})|q]\times n_>\left(\left|\mathbf{q}+\frac{1}{2}\mathbf{P}\right|\right)n_>\left(\left|\mathbf{q}-\frac{1}{2}\mathbf{P}\right|\right). \tag{A9}$$

Taking into account the identity

$$e^{-\beta E_{\mathbf{qP}}}n_>\left(\left|\mathbf{q}+\frac{1}{2}\mathbf{P}\right|\right)n_>\left(\left|\mathbf{q}-\frac{1}{2}\mathbf{P}\right|\right)=n\left(\left|\mathbf{q}+\frac{1}{2}\mathbf{P}\right|\right)n\left(\left|\mathbf{q}-\frac{1}{2}\mathbf{P}\right|\right), \tag{A10}$$

Eq. (A9) reduces to the finite temperature Brueckner expression of Eq. (10) in the text. In the calculations we adopt the angular average approximation for the entry energy only for the higher order terms, since for the first term the integration can be easily done numerically. This term, which corresponds to Eq. (10) of Sec. II, has the explicit form

$$\omega_1=\frac{\Omega_1}{V}=\frac{1}{8\pi^2\rho}\sum_{lSJT}\hat{T}^2\hat{J}^2\int_0^{+\infty}k_1^2dk_1\int_0^{+\infty}k_2^2dk_2\int d(\cos\theta)\times[ql|K^{JST}(\omega,P)|ql]n(k_1)n(k_2), \tag{A11}$$

where $q=|\mathbf{k}_2-\mathbf{k}_1|/2$, $P=|\mathbf{k}_2+\mathbf{k}_1|$, $\omega=e_{k_1}+e_{k_2}$, and θ is the angle between the single-particle momenta $\mathbf{k}_1$ and $\mathbf{k}_2$.

APPENDIX B

In this appendix we discuss the problem of the fulfillment of the Hughenholtz–Van Hove (HVH) theorem in the calculation of the pressure and other thermodynamical quantities. The theorem indicates which diagrams in the perturbation expansion should be selected in order to satisfy consistently the thermodynamical relation

$$\mu=f+p/\rho, \tag{B1}$$

where f is the free energy per particle and p the pressure. In a general microscopic treatment one has to check if this relation is violated. In the present context the constraint required by the theorem is equivalent to demanding that the pressure calculated directly from the grand-canonical potential, $\tilde{p}=-\omega$, be equal to the pressure calculated from the free energy, $p=\rho^2\partial f/\partial\rho$. At the level of the finite temperature Brueckner approximation, the two procedures of extracting the pressure give different results. This difference can be ascribed directly to a well-defined self-energy diagram, the so-called ''rearrangement term'' [18], which is absent in the standard Brueckner approximation adopted here. This can be seen easily by noticing that the fulfillment of the theorem be equivalent also to demand that the chemical potential extracted from the free energy, $\mu=\partial F/\partial N$, is equal to the chemical potential $\tilde{\mu}$ extracted from the density according to Eq. (19), which in the present scheme is used to derive the free energy F from the grand-canonical potential Ω. In fact,

$$\mu=\frac{\partial F}{\partial N}=f+\rho\left(\frac{\partial f}{\partial\rho}\right)=f+\rho[-f+\tilde{\mu}]/\rho\equiv\tilde{\mu}. \tag{B2}$$

It can be shown that it is possible to reconcile the Brueckner theory with the HVH theorem if one adopts as a definition of the pressure the one calculated from the derivative of the free energy and the chemical potential is taken equal to μ. Let us in fact modify the single-particle potential $U(k)$ by adding a constant shift $\Delta\mu=\mu-\tilde{\mu}$. Then Eq. (19) is unaffected, provided we redefine the chemical potential as μ, and the unperturbed grand-canonical potential $\Omega_0{}'$ is changed to $\Omega_0{}''=\Omega_0{}'+\Delta\mu N$. Therefore, from Eq. (16) one gets

$$\Omega_0{}'+\tilde{\mu}N=\Omega_0{}''+\mu N\equiv F_0 \tag{B3}$$

and the unperturbed Free energy F_0 remains unaffected. Of course, the shift $\Delta\mu$ in the single-particle potential will in general modify the Brueckner G matrix and therefore the interacting part $\Delta\Omega$ of the grand-canonical potential. However, it has been shown that, at zero temperature, the Brueckner energy is actually stable, since one has to include consistently in the calculation also the modification of the lower diagram in Fig. 4(b). In fact, once the single-particle potential has been shifted, this diagram is not any more exactly canceled out by the corresponding lower diagram of Fig. 4(d). It has been shown that indeed the correction compensates quite accurately the modification of the Brueckner energy [47]. Indeed, one can verify analytically that the correc-

tion of the U insertion diagram is just equal to the opposite of the first order correction to the Brueckner energy.

We have seen that the main modification introduced by the temperature is described by the NTBBG prescription. Therefore, the above consideration about the stability of the Brueckner energy can be extended safely to finite temperatures.

In conclusion, the procedure we are proposing is to adopt for the pressure the definition $p=\rho^2\partial f/\partial\rho$, with f calculated as described in Sec. II, for the chemical potential $\mu=\partial F\partial N$, without modifying the Brueckner energy. The HVH theorem is then automatically fulfilled. A similar procedure was suggested by Heyer *et al.* [48] in the case of the finite temperature EOS extracted from phenomenological forces.

APPENDIX C

In this appendix we give some details about the procedure used to reduce the original three-body forces to an effective two-body one. This effective force is obtained [23] by averaging the interaction of Eq. (C1) over the spin and isospin of the particle j and folding over the coordinate $\mathbf{r}_j$ of particle j with the product of the two-body correlation functions $[1-g(r_{ij})]^2$ and $[1-g(r_{jk})]^2$, which expresses the probability of finding particle j at the distances r_{ij} from particle i and at the distance r_{jk} from particle k in the medium,

$$v_3^{\rm eff}(r_{ik})=\rho\sum_{\sigma_j,\tau_j}\int d^3r_j V_{ijk}[1-g(r_{ij})]^2[1-g(r_{jk})]^2, \tag{C1}$$

where ρ is the density. The correlation functions should be in principle calculated self-consistently from the Brueckner G matrix at each density and temperature,

$$\Psi(\mathbf{r})=[1-g(\mathbf{r})]\cdot\phi(\mathbf{r}),$$

$$g(\mathbf{r})=-\left\langle \mathbf{r}\left|\frac{Q}{e}G\right|k_1k_2\right\rangle, \tag{C2}$$

where Ψ is the two-body relative wave function in the medium, ϕ the corresponding unperturbed wave function, and e the proper energy denominator. Unfortunately this is in practice a very lengthy task to achieve. However, it turns out that both the density and temperature dependence in the relevant region are very small, as illustrated in Fig. 5, where the correlation function is plotted for $k_1=k_2\approx 0$ in the $^1S_0$ channel. As one can see, the correlation functions are characterized by a sharp decrease to 0 at small distances and a rapid increase to 1 at larger distances. This trend is almost independent of the density and initial momenta, certainly due to the influence of the strong repulsion of the NN core, which is of the order of 1 GeV and therefore much larger than the relevant Fermi energies. Since the only contribution to the wave function at short distances comes from S waves, it is enough to construct the correlation function from these channels only. Figure 5 also suggests a simplified form for the correlation functions to be used in Eq. (C1), namely, a step function at a suitable radius. This is the approximation we used in the actual applications. We have checked that the results are insensitive to the detailed form of the correlation and to small variations of the radius of the step function. This insensitivity is due to the three-dimensional integration in $\vec{r}_{jk}$ in Eq. (3) which smooths out the details of the correlation function at small distances. Notice, anyhow, that still a strong density dependence remains, due to the ρ factor in Eq. (C1).

For nuclear matter and neutron matter only the anticommutator term contributes to the averaging of the $V^{2\pi}$, because of symmetry arguments. After averaging over spin and isospin of the third particle and using the relation $\mathbf{r}_{jk}=\mathbf{r}_{ik}+\mathbf{r}_{ij}$, the explicit form of the two form factors v_S and v_T of Eq. (30) reads

$$v_S(r_{ik})=2\pi A\rho\int r_{jk}^2dr_{jk}\int d(\cos\theta)[1-g(r_{ji})]^2[1-g(r_{jk})]^2$$
$$\times\left[Y(r_{ji})Y(r_{jk})+\left(\frac{3}{2}\frac{r_{ij}^2+r_{jk}^2-r_{ik}^2}{r_{ji}^2}-1\right)T(r_{ji})T(r_{jk})-3T(r_{jk})T(r_{ji})\frac{r_{ik}(\mathbf{r}_{ji}\cdot\mathbf{r}_{jk})}{r_{jk}r_{ji}^2}\mathrm{P}_1(\cos\theta)\right],$$

$$v_T(r_{ik})=2\pi A\rho\int r_{jk}^2dr_{jk}\int d(\cos\theta)[1-g(r_{ji})]^2[1-g(r_{jk})]^2T(r_{jk})$$
$$\times\left\{2\mathrm{P}_2(\cos\theta)Y(r_{ji})+T(r_{ji})\left[\mathrm{P}_2(\cos\theta)\left(\frac{(3\mathbf{r}_{ji}\cdot\mathbf{r}_{jk})}{r_{ji}^2}-2\right)-3\mathrm{P}_1(\cos\theta)\frac{r_{ik}(\mathbf{r}_{ji}\cdot\mathbf{r}_{jk})}{r_{jk}r_{ji}^2}\right]\right\}, \tag{C3}$$

where the z axis was taken along the vector $\mathbf{r}_{ik}$, and $P_l(\cos\theta)$ are the Legendre polynomials of order l. These two-dimensional integrations can be easily done numerically. The repulsive scalar part of Eq. (29) gives obviously a scalar repulsive effective two-body force when the integration over the third particle coordinates is performed.

[1] J. Pochodzalla *et al.*, Phys. Rev. Lett. **75**, 1040 (1995).
[2] Y. G. Ma *et al.*, Phys. Lett. B **390**, 41 (1997).
[3] For an up-to-date review see, for example, *Proceedings of the Internernational Conference ''CRIS 96,''* edited by S. Costa, S. Albergo, A. Insolia, and C. Tuvé (World Scientific, Singapore, 1996).
[4] G. Sauer, M. Chandra, and U. Mosel, Nucl. Phys. **A264**, 221 (1976).
[5] J. Bondorf *et al.*, Phys. Rep. **257**, 133 (1995), and references therein.
[6] D. H. E. Gross *et al.*, Phys. Rep. **279**, 119 (1997), and references therein.
[7] B. Friedman and V. R. Pandharipande, Nucl. Phys. **A361**, 502 (1981).
[8] M. Baldo, I. Bombaci, L. S. Ferreira, and U. Lombardo, Nucl. Phys. **A583**, 599c (1995).
[9] C. Das and R. K. Tripathi, Phys. Rev. C **45**, 2217 (1992); R. K. Tripathi, Phys. Lett. **101B**, 369 (1981); Phys. Rev. C **25**, 1114 (1982).
[10] Claude Bloch, Nucl. Phys. **7**, 451 (1958); Claude Bloch and Cyrano De Dominicis, *ibid.* **7**, 459 (1958); **10**, 181 (1959); **10**, 509 (1959).
[11] B. Day, Phys. Rev. C **24**, 1203 (1981); Phys. Rev. Lett. **47**, 226 (1981); B. Day and R. B. Wiringa, Phys. Rev. C **32**, 1057 (1985).
[12] A. L. Fetter and J. D. Walecka, *Quantum Theory of Many Particle Physics* (McGraw-Hill, New York, 1971).
[13] For a recent review, see P. A. Hening, Phys. Rep. **253**, 235 (1995).
[14] K. A. Brueckner and J. L. Gammel, Phys. Rev. **109**, 1023 (1958).
[15] M. Baldo and L. S. Ferreira, Nucl. Phys. **A569**, 645 (1994).
[16] H. Q. Song, M. Baldo, G. Giansiracusa, and U. Lombardo, Phys. Lett. B **411**, 237 (1997); Phys. Rev. Lett. **81**, 1584 (1998).
[17] J. Goldstone, Proc. R. Soc. London, Ser. A **239**, 267 (1957).
[18] J. P. Jeukenne, A. Lejeune, and C. Mahaux, Phys. Rep. **25**, 83 (1976).
[19] H. A. Bethe, B. H. Brandow, and A. G. Petschek, Phys. Rev. **129**, 225 (1962).
[20] D. J. Thouless, *The Quantum Mechanics of Many-Body Systems* (Academic Press, New York, 1961), Chap. VII, Sec. 3.
[21] *Nuclear Methods and the Nuclear Equation of State*, edited by M. Baldo (World Scientific, Singapore, 1998), Chap. I.
[22] M. Baldo, I. Bombaci, L. S. Ferreira, G. Giansiracusa, and U. Lombardo, Phys. Rev. C **43**, 2605 (1991).
[23] A. Lejeune, P. Grangé, M. Martzolff, and J. Cugnon, Nucl. Phys. **A453**, 189 (1986).
[24] N. M. Hughenholtz and L. Van Hove, Physica (Amsterdam) **24**, 363 (1958).
[25] J. F. Mathiot, Phys. Rep. **173**, 63 (1989).
[26] J. Carlson, V. R. Pandharipande, and R. B. Wiringa, Nucl. Phys. **A401**, 59 (1983); R. Schiavilla, V. R. Pandharipande, and R. B. Wiringa, *ibid.* **A449**, 219 (1986).
[27] P. Grangé, A. Lejeune, M. Martzolff, and J. F. Mathiot, Phys. Rev. C **40**, 1040 (1989).
[28] R. B. Wiringa, R. A. Smith, and T. L. Ainsworth, Phys. Rev. C **29**, 1207 (1984).
[29] M. Brack and P. Quentin, Phys. Lett. **52B**, 159 (1974).
[30] I. Bombaci, T. T. S. Kuo, and U. Lombardo, Phys. Rep. **242**, 165 (1994).
[31] B. ter Haar and R. Malfliet, Phys. Rev. Lett. **56**, 1237 (1986); Phys. Rep. **149**, 207 (1987).
[32] H. Huber, F. Weber, and M. K. Weigel, nucl-th/9803026, 1998.
[33] R. Machleidt, Adv. Nucl. Phys. **19**, 189 (1989).
[34] L. P. Csernai and J. I. Kapusta, Phys. Rep. **131**, 223 (1986).
[35] G. Q. Li, R. Machleidt, and R. Brockmann, Phys. Rev. C **45**, 2782 (1992).
[36] G. E. Brown, W. Weise, G. Baym, and J. Speth, Comments Nucl. Part. Phys. **17**, 39 (1987).
[37] I. Bombaci and U. Lombardo, Phys. Rev. C **44**, 1892 (1991).
[38] A. de Shalit and H. Feshbach, *Theoretical Nuclear Physics* (Wiley, New York, 1974), Vol. I.
[39] H. A. Bethe, G. E. Brown, J. Applegate, and J. M. Lattimer, Nucl. Phys. **A324**, 487 (1979).
[40] E. Baron, J. Cooperstein, and S. Kahana, Phys. Rev. Lett. **55**, 126 (1985).
[41] See for instance H. Th. Janka and E. Müller, in *Supernovae and Supernova Remnants*, edited by R. McCray and Z. Wang (Cambridge University Press, Cambridge, England, 1996), and references therein.
[42] H. A. Bethe and J. R. Wilson, Astrophys. J. **295**, 14 (1985).
[43] S. Levit and P. Bonche, Nucl. Phys. **A437**, 426 (1985).
[44] H. Q. Song and R. K. Su, Phys. Rev. C **44**, 2505 (1991).
[45] M. Baldo, Y. H. Cai, G. Giansiracusa, U. Lombardo, and H. Q. Song, Phys. Lett. B **340**, 13 (1994).
[46] T. Suomijiarvi *et al.*, Phys. Rev. C **53**, 2258 (1996), and references therein.
[47] R. Sartor (private communication).
[48] J. Heyer, T. T. S. Kuo, J. P. Shen, and S. S. Wu, Phys. Lett. B **202**, 465 (1988).